BMC Microbiology

RESEARCH

Open Access

Lactobacillus Johnsonii YH1136 alleviates schizophrenia-like behavior in mice: a gut–microbiota–brain axis hypothesis study

Liqin Zheng[1,5†], Jinge Xin[2†], Huiqian Ye[4†], Ning Sun[3], Baoxing Gan[3], Xuemei Gong[3], Shusheng Bao[1,5], Min Xiang[4], Hesong Wang[2], Xueqin Ni[3], Hao Li[4*] and Tao Zhang[1,5*]

Abstract

Based on the microbiota–gut–brain axis (MGBA) hypothesis, probiotics play an increasingly important role in treating various psychiatric disorders. Schizophrenia (SCZ) is a common mental disease with a complex pathogenesis and is challenging to treat. Although studies have elucidated the mechanisms associated with the interactions between the microbiota–gut–brain axis and SCZ, few have specifically used probiotics as a therapeutic intervention for SCZ. Accordingly, the current study determines whether *L. johnsonii* YH1136 effectively prevents SCZ-like behavior in mice and identifies the associated key microbes and metabolites. An SCZ mouse model was established by intraperitoneal injection of MK-801; *L. johnsonii* YH1136 was administered via oral gavage. *L. johnsonii* YH1136 significantly improves abnormal behaviors, including psychomotor hyperactivity and sociability and alleviates aberrant enzyme expression associated with tryptophan metabolism in SCZ mice. Additionally, *L. johnsonii* YH1136 upregulates hippocampal brain-derived neurotrophic factor (BDNF) levels while downregulating tryptophan 2,3-dioxygenase (TDO2), indoleamine-pyrrole 2,3-dioxygenase 1 (IDO1), kynurenine aminotransferase 1 (KAT1). Subsequent 16S rRNA sequencing of intestinal contents suggests that *L. johnsonii* YH1136 modulates the gut flora structure and composition by increasing the relative abundance of *Lactobacillus* and decreasing *Dubosiella* in SCZ mice. N-acetylneuraminic acid and hypoxanthine are the key serum metabolites mediating the interaction between the MGBA and SCZ. These results partially reveal the mechanism underlying the effects of *L. johnsonii* YH1136 on SCZ-like behavior in mice, supporting the development of therapeutic *L. johnsonii* probiotic formulations against SCZ.

Keywords Schizophrenia, Psychobiotics, Multi-omics, Microbiota–gut–brain axis, *Lactobacillus johnsonii*

†Liqin Zheng, Jinge Xin and Huiqian Ye are equal contributors.

*Correspondence:
Hao Li
727386441@qq.com
Tao Zhang
tao.zhang@uestc.edu.cn
[1] School of Life Science and Technology, High-Field Magnetic Resonance Brain Imaging Key Laboratory of Sichuan Province, University of Electronic Science and Technology of China, Chengdu, China
[2] Baiyun Branch, Nanfang Hospital, Southern Medical University, Guangzhou, China
[3] Animal Microecology Institute College of Veterinary Medicine, Sichuan Agricultural University, Chengdu, China
[4] The Fourth People's Hospital of Ya'an, 7 Qingxi Road Ya'an 625000, Yucheng ZoneSichuan, China
[5] MOE Key Lab for Neuroinformation, Sichuan Institute for Brain Science and Brain-Inspired Intelligence, University of Electronic Science and Technology of China, 2006 Xiyuan Avenue, West Hi-Tech Zone, Chengdu, Sichuan 611731, China

Introduction

The gut microbiota, actively engaged with the host from birth, orchestrates essential physiological functions including immune regulation, metabolic homeostasis, and neurodevelopment, thereby constituting a fundamental component of host physiology. In recent years, mounting evidence has increasingly recognized the pivotal role of gut microbial communities in the pathogenesis of cognitive impairment and psychiatric disorders. The microbiota–gut–brain axis (MGBA) is a bidirectional pathway that indicates the interaction between the gut microbiota and the brain [1, 2]. Based on the MGBA, the gut microbiota can affect individual behavior through neural, endocrine, and immune pathways, also impacting the occurrence of mental diseases, such as depression and anxiety [3, 4]. The gut microbiota exhibits dynamic compositional diversity throughout host ontogeny. Within this ecosystem, beneficial live microorganisms that confer health advantages are formally defined as probiotics. A homeostatic gut microbial community mitigates disease susceptibility through two primary mechanisms: (1) competitively inhibiting pathogen colonization by promoting the proliferation of commensal symbionts, and (2) synthesizing bioactive metabolites (e.g., short-chain fatty acids, neurotransmitters) that systemically regulate host physiology [5, 6]. Indeed, the use of probiotics to improve intestinal microflora is expected to become a new and effective method for alleviating mental disorders [7]. Accordingly, the concept of psychobiotics was introduced in 2013 [8], describing a subclass of probiotics that can interact with an individual's symbiotic gut microbes to exert positive psychiatric effects in animal models or patients when ingested in appropriate quantities [9].

Schizophrenia (SCZ) is a severe mental disease with high recurrence, disability, and suicide rates, affecting approximately 1% of the global population [10, 11]. The high heterogeneity and complex pathological mechanisms of SCZ have considerably impacted treatment efficacy, with approximately one-third of all patients showing no response to antipsychotics [12, 13]. A recent increase in studies investigating the relationship between SCZ and MGBA has provided new perspectives for preventing and alleviating SCZ symptoms. For example, Thirion et al., through metagenomic profiling, revealed that the intestinal microbial diversity and composition of patients with SCZ differ significantly from those of healthy controls or patients with metabolic syndrome. Moreover, the cognitive impairment of SCZ are associated with gut microbe biosynthesis of tyrosine [14]. Similarly, in a multi-omics study, Wang et al. studied the effects of genes, metabolism, and gut microbiota on brain function and their relationship in patients with SCZ, further identifying a strong correlation between SCZ and MGBA. They found that the altered metabolites and microbiome are associated with neuroactive metabolites (e.g., gamma-aminobutyric acid). Specifically, gray matter volume and functional connectivity disturbances mediate the relationships between gut microbes and symptom severity as well as the relationships between microbes, metabolites (e.g., l-2,4-diaminobutyric acid), and cognitive function [15].

The effects of probiotic supplementation have also been investigated in patients with SCZ. For example, Tomasik et al. reported that supplementation with probiotics (a mixture of *Lactobacillus rhamnosus* and *Bifidobacterium animalis*) for 14 weeks combined with antipsychotics significantly alters the levels of related proteins and contributes to the regulation of immune and intestinal epithelial cells through the interleukin (IL)−17 family of cytokines. However, no changes were observed in the Positive and Negative Syndrome Scale (PANSS) psychiatric symptom scores [16]. Meanwhile, another study reported an improvement in anxiety, depression, and PANSS scores after treatment with probiotics *(Bifidobacterium breve*) in patients with SCZ for four weeks; the associated mechanism involves IL-22 and tumor necrosis factor (TNF)-related activation-induced cytokines associated with gut epithelial barrier function [17]. However, whether probiotic supplementation prevents and modulates SCZ symptoms via MGBA remains unclear.

L. johnsonii YH1136 (CCTCC M 20221116) was isolated from the feces of a young, healthy Tibetan girl from the Nagqu region at an altitude of 5,000 m. We previously reported that *L. johnsonii* YH1136 prevents microbiome dysregulation in high-altitude-exposed mice and promotes repair of the intestinal barrier by reshaping the intestinal microbiota, reducing the abundance of pathogenic bacteria, and regulating the expression of target genes associated with miRNAs in the ileum [18]. *L. johnsonii* YH1136 can also effectively reduce the blood uric acid concentration in hyperuricemic mice, increase uric acid excretion, inhibit the inflammatory response in the kidneys, and repair kidney damage in hyperuricemic mice [5]. Moreover, *L. johnsonii* regulates MGBA and improves intestinal and brain functions. Lee et al. found that oral administration of *L. johnsonii* CJLJ103 enhances the performance of passive avoidance and Y-maze tasks in mice, increases brain-derived neurotrophic factor (BDNF) and TNF-α expression, inhibits nuclear factor kappa-B activation in the hippocampus, and alleviates scopolamine-induced memory impairment [19]. The *L. johnsonii* BS15 also improves the intestinal environment by alleviating intestinal inflammation, enhancing intestinal physiological functions and permeability, and protecting the hippocampal memory function by increasing neurotransmitter levels and antioxidant levels in mice

[20, 21]. Additionally, oral administration of *L. johnsonii* improves brain functions related to memory through MGBA. However, there is insufficient evidence that *L. johnsonii* administration prevents and alleviates SCZ symptoms.

Therefore, the current study evaluates whether *L. johnsonii* YH1136 can be applied as a psychobiotic with mental health and cognitive behavior benefits. The primary questions are: (1) Does *L. johnsonii* YH1136 effectively prevent SCZ-like behavior in mice?; (2) What are the possible key microbes and metabolites involved? To this end, a SCZ model was created in C57/BL mice via administration of the noncompetitive N-methyl-d-aspartate receptor (NR) antagonist MK-801.

Materials and Methods

Culture and treatment with *Lactobacillus johnsonii* YH1136

The *L. johnsonii* YH1136 (CCTCC M 20221116) was isolated from the feces of a young, healthy Tibetan girl from the Nagqu region at an altitude of 5,000 m, and then cultured in de Man, Rogosa, and Sharpe (MRS) broth at 37 ℃. The plate count method was used to count the cells. Briefly, bacteria solution was diluted using a tenfold gradient with phosphate-buffered saline (PBS). The dilution 10^{-5}, 10^{-6}, and 10^{-7} dilutions were selected and added dropwise (10 μL) to the MRS agar in triplicate. The MRS agar was cultured for 36 h at 37 ℃ and then counted the bacteria colonies. Subsequently, the cells were centrifuged (3000 rpm, 4 ℃, 15 min), washed, and resuspended in PBS (pH 7.0) for experimental use. The concentration of the final suspension was 1×10^9 colony forming units (CFU) YH1136/mL (daily consumption dose: 0.2 mL/mouse) [5, 18].

Animals

A total of 66 male C57BL/6 mice (8 weeks old) purchased from Si Pei Fu Biotechnology Co., Ltd. (Beijing, China). The animals were raised with 12-h light/dark cycle, a constant temperature (25 ± 2.0 ℃) and humidity (55 ± 10%), and provided food and water ad libitum. All experiments were conducted in accordance with the Guidelines for the Care and Use of Laboratory Animals and were approved by the Institutional Animal Care and Use Committee of Sichuan Agricultural University (approval number: SYXKchuan2019-187).

Experimental design

After one week of acclimatization, the mice were randomly divided into three groups ($n=22$ mice/group): control (Ctrl), SCZ model (SCZ), and probiotic (SCZ-P) groups. In the SCZ-P group, each mouse was administered 0.2 mL of 1×10^9/mL YH1136 CFU daily for six weeks by gavage. In the Ctrl and SCZ groups, each mouse was administered 0.2 mL saline daily for six weeks by gavage. From the fifth week, the SCZ and SCZ-P groups were intraperitoneally injected with MK-801 (0.6 mg/kg, IM0300, Beijing Solarbio Science & Technology Co., Ltd.) for two weeks to establish the SCZ mouse model [22], while mice in the Ctrl group were intraperitoneally injected with saline (0.6 mg/kg, pH 7.0) as a substitute.

Three behavioral tests related to SCZ were performed after established the SCZ mouse model. Twenty-four hours after completing all behavioral tests, blood was collected from the orbital vein of the mice, then the mice were immediately sacrificed through cervical dislocation. The brain and the contents of the ileal and colonic segment were collected. Serum was separated from blood by centrifuged at 3000 rpm for 15 min at 4 °C after letting stand at room temperature for two hours. The intestinal contents were initially stored on ice and immediately transferred to −80 °C. Tissues were washed with ice cold RNase-free water and blotted with absorbent paper, after which they were immediately stored at −80 °C.

Behavioral testing

Behavioral tests were performed on 12 mice per group randomly selected. Animals were given 1 h of habituation in the behavioral testing room before testing to minimize novelty or stress effects. Behavioral tests were performed in the following order: (1) elevated plus maze test (EPMT), (2) open field test (OFT), and (3) three-chamber sociability test (TCST). All tests were performed as previously described with minor modifications (i.e., the size of the experimental instrument was carried out according to the actual situation) [23–25]. Tests were recorded using a video-computerized tracking system (SMART 3.0; Panlab SL, Barcelona, Spain) or evaluated separately by two experienced researchers via manual observation. The investigators were blinded to the treatment conditions of the mice during experiments and outcome assessments. All objects used for the tests were cleaned with 70% ethanol between each trial, and feces and urine in the box were removed.

Real-time quantitative PCR (RT-qPCR) detection of mRNA expression levels

To measure the mRNA levels of *Bdnf*, tryptophan-2,3-dioxygenase 2 (*Tdo2*), indoleamine 2,3-dioxygenase (*Ido*) 1–2, kynurenine aminotransferases (*Kat*) 1–4, tryptophan hydroxylase 1 (*Tph1*), *Nr*1, *Nr*2A, *Nr*2B, and β-actin (*Actb*) [26–28], the E.Z.N.A.® Total RNA Kit (OMEGA BioTek, Doraville, GA, USA) was used to isolate total RNA from the hippocampal and prefrontal cortex (PFC) tissues. The Prime Script RT kit with gDNA eraser (Thermo Scientific, Waltham, MA, USA) was used to synthesize first-strand complementary DNA (cDNA).

The forward and reverse primer sequences (Hangzhou Youkang Biotechnology Co., Ltd., Zhejiang, China) used in this study are presented in Table 1. Following the manufacturer's instructions, cDNA, synthetic primers, SYBR Green Supermix (Bio-Rad, Hercules, CA, USA), and RT-qPCR were performed using a LightCycle R96 Real-Time System (Boehringer Mannheim GmbH, Germany). The RT-qPCR conditions were as follows: initial 50 °C for 2 min, followed by 95 °C for 5 min, denaturation at 95 °C for 10 s, and annealing at the optimal temperature for 30 s for 40 cycles. *Actb* was used as a reference gene to normalize the relative mRNA expression levels of the target genes, with values presented as $2^{-\Delta\Delta Ct}$ [29].

Immunofluorescence staining

The brain was removed from each mouse, fixed with 4% paraformaldehyde solution, and stored in 4 ℃. Tissues were embedded in paraffin and cut using a microtome (Wuhan Servicebio Technology Co., Ltd., Hubei, China, i.e. Servicebio). After dewaxing and hydration, the sections were repaired using with EDTA antigen repair solution (pH 8.0 or pH 9.0; G1206, G1203, Servicebio). After natural cooling, the slides were placed in PBS (pH 7.4) and washed thrice by shaking on a decolorizing shaker for 5 min each. After the sections were slightly dried, circles were drawn around the tissue with a tissue pen, and 3% bovine serum albumin was added for 30 min to seal the sections. Sections were then incubated overnight at 4 ℃ with polyclonal rabbit anti-TDO2 antibody (1:100, 15,880–1-AP, Proteintech), polyclonal rabbit anti-IDO1 antibody (1:100, 13,268–1-AP, Proteintech), polyclonal rabbit anti-IDO2 antibody (1:200, bs-16640R, Bioss), polyclonal rabbit anti-TPH1 antibody (1:50, BS3727, Bioworld), or polyclonal rabbit anti-KAT1 antibody (1:500, GB11906, Servicebio). The slides were placed in PBS (pH 7.4) and washed thrice by shaking on a decolorizing shaker, 5 min each. A corresponding CY3-labeled goat anti-rabbit IgG was added and incubated at room temperature for 50 min in the dark. Subsequently, the slides were placed in PBS (pH 7.4) and washed by shaking on a decolorizing shaker thrice, 5 min each. The nuclei were re-stained with 4',6-diamidino-2-phenylindole (DAPI) solution and incubated at room temperature for 10 min in the dark. Confocal micrographs were collected on OLYMPUS microscope.

Table 1 Primer sequences for RT-qPCR in hippocampus and PFC

Gene	Sequence (5′−3′)	Reference
β-actin	Forward: GCTCTTTTCCAGCCTTCCTT Reverse: GATGTCAACGTCACACTT	Xin. et al. 2020 [25]
BDNF	Forward: GCGCCCATGAAAGAAGTAAA Reverse: TCGTCAGACCTCTCGAACCT	Xin. et al. 2020 [25]
TDO2	Forward: AGGAACATGCTCAAGGTG ATAGC Reverse: CTGTAGACTCTGGAAGCCTGAT	Zhu. et al. 2019 [26]
IDO1	Forward: CAAAGCAATCCCCACTGTATCC Reverse: ACAAAGTCACGCATCCTCTTAAA	Zhu. et al. 2019 [26]
IDO2	Forward: CCTCATCCCTCCTTCCTTTC Reverse: GGAGCAATTGCCTGGTATGT	Zhu. et al. 2019 [26]
KAT1	Forward: CGAAGGCTGGAAGGGATCG Reverse: GCGGTGAGAAGTCAGGGAA	Zhu. et al. 2019 [26]
KAT2	Forward: ATGAATTACTCACGGTTCCTCAC Reverse: AACATGCTCGGGTTTGGAGAT	Zhu. et al. 2019 [26]
KAT3	Forward: TTCAAAAACGCCAAACGAATCG Reverse: GATGACCAAAGCCTCTTGTGT	Zhu. et al. 2019 [26]
KAT4	Forward: GGACCTCCAGATCCCATCCT Reverse: GGTTTTCCGTTATCATCCCGGTA	Zhu. et al. 2019 [26]
TPH1	Forward: AACAAAGACCATTCCTCC GAAAG Reverse: TGTAACAGGCTCACATGATTCTC	Zhu. et al. 2019 [26]
NR1	Forward: TGACCCAGGAACCAAGAATG Reverse: CTTGCCGTTGATTAGCTGAAG	Areal. et al. 2017 [27]
NR2A	Forward: ATGACTATTCTCCGCCTTTCC Reverse: AGTTTACAGCCTTCATCCCTC	Areal. et al. 2017 [27]
NR2B	Forward: GAACGAGACTGACCCAAAGAG Reverse: CAGAAGCTTGCTGTTCAATGG	Areal. et al. 2017 [27]

16S rRNA gene sequencing and analysis

A total of 200 μL (final elution volume) of ileal or colonic DNA samples were extracted using the E.Z.N.A.TM fecal DNA extraction kit (OMEGA Bio-Tek, Norcross, GA, USA). After measuring DNA quality and integrity via agarose gel electrophoresis and a NanoDrop NC2000 spectrophotometer (Thermo Fisher Scientific, Waltham, MA, USA), the extracted DNA was sent to Shanghai Personal Biotechnology Co., Ltd. (Shanghai, China). The specific barcode was combined into the amplification primers, and PCR amplification and pair-end 2×250 bp sequencing of the bacterial 16S rRNA gene were performed using the Illumina MiSeq sequencing platform and the V3–V4 region fragment. The primer sequences were: 338F 5'-ACTCCTACGGGAGGCAGCA-3' and 806R 5'-GGA CTACHVGGGTWTCTAAT-3'. The reaction volume comprised buffer (5×, 5 μL), FastPfu DNA polymerase (5 U/μL, 0.25 μL), dNTPs (2.5 mM, 2 μL), forward and reverse primers (10 μM, 1 μL), DNA template (1 μL) and ddH_2O (14.75 μL). The amplification procedure consisted of an initial denaturation at 98 ℃ for 5 min, degeneration at 98 ℃ for 30 s with 25 cycles, annealing at 53 °C for 30 s, extension at 72 °C for 45 s, and a final extension at 72 °C for 5 min. PCR amplicons were purified and quantified using Vazyme VAHTSTM DNA Clean Beads (Vazyme, Nanjing, China) and the Quant-iT PicoGreen dsDNA Assay Kit (Invitrogen, Carlsbad, CA, USA).

Sequence and bioinformatics analysis

Bioinformatics analysis of the sequencing data was performed using QIIME2 (https://docs.qiime2.org) [30]. The

demux, cutadapt, and DADA2 plugins [31] were used to demultiplex raw data, cut primers, and perform quality filtering, denoising, merging, and sequence removal. The non-singleton amplicon sequence variants (ASVs) were aligned with 'mafft', and later used to construct a phylogenetic relationship using fasttree2 [32]. Finally, the species in the abundance table were annotated using the feature-classifier plugin based on the Navier-Bayes classifier and the SILVA 138 database [33].

The alpha diversity index of intestinal flora in the ileum and colon was calculated using the Chao1 and Shannon diversity indices to assess differences in microbial richness and diversity [34]. Beta diversity analysis investigates the similarity in community structure between different samples. Based on the Bray–Curtis [35], principal coordinate analysis (PCoA) [36] was used to visually analyze the composition and structure of the intestinal microbial community. To reveal changes in intestinal flora composition after ingesting YH1136, high-abundance (relative abundance > 1%) microbial taxa were clustered at the phylum and genus levels in each group. The Wilcoxon rank-sum test was used to compare specific microbial taxa. According to Dai et al. [37], microbial taxa were divided into six groups based on relative abundance: (i) rare taxa (RT), ASV with abundance ≤ 0.1% in all samples; (ii) abundant taxa (AT), abundance ≥ 1% in all samples; (iii) moderate taxa (MT), abundance > 0.1% and < 1% in all samples; (iv) conditionally rare taxa (CRT) abundance < 1% in all samples, and < 0.1% in some samples; (v) conditionally abundant taxa (CAT) abundance > 0.1% in all samples and > 1% ASV in some samples; (vi) conditionally rare or abundant taxa (CRAT), abundance spans the ASV from rare (minimum abundance ≤ 0.1%) to abundant (maximum abundance ≥ 1%).

To identify the key intestinal species impacted by *L. johnsonii* YH1136 intake that play important roles in preventing or alleviating SCZ symptoms, species that were detected in very low abundance or only appeared in a limited number of samples were excluded. This reduced the complexity of network analysis and improved the efficiency of locating the most critical species in the community. ASVs that occurred in eight samples (minimum number of repeats for different treatments) with a > 50% occurrence rate and at least two sequences (avoiding single-count ASVs) were retained as the primary objects for screening key species. Subsequently, the indicator species analysis method [38] was employed to calculate the bicolumn correlation coefficient (r) of a point where ASV was positively correlated with one treatment; $P < 0.05$ was set as the screening threshold, and the bicolumn network graph was obtained according to gate level coloring. In addition, the specificity and occupancy (SPEC-OCCU) of the ASVs was calculated to select feature species from different groups, and SPEC-OCCU plots [39] were constructed to identify potential key species (specificity and occupancy > 0.7). The key species closely related to *L. johnsonii* YH1136 intake were screened based on the indicator species and specificity-share results of these analyses.

Notably, a computational method suitable for the characteristics of high-throughput omics data was selected, namely molecular ecological network analysis (MENA) [40] to clarify species co-occurrence patterns in microbial communities under different treatments and their responses to environmental changes. A microbial species interaction network was constructed. Based on the cohesiveness and topological properties of the network, nodes were defined as important for maintaining the stability of the network structure, while their absence may lead to the decomposition of network modules and networks. The Levins niche overlap index (NOI) [41] of each key treatment species was calculated, and relationship pairs with a NOI > 0.5 were presented. The bootstrap method was used to randomly rearrange the species abundance table and to calculate the zero distribution and confidence interval of the NOI among these species to further evaluate the intensity of niche overlap among key species. Finally, the PICRUSt2 tool [42] was employed to perform 16S species annotation, copy number homogenization, hidden state prediction of gene families, genome function inference, and functional pathway abundance prediction; the ggpicurst2 function was used to analyze and visualize the prediction function of different groups.

Serum metabolomics

Serum samples from each group were sent to Shanghai Personal Biotechnology Co. Ltd. (Shanghai, China) for untargeted metabolomic analyses. After the samples were slowly thawed at 4 ℃, appropriate amounts of samples were added to pre-cooled methanol/acetonitrile/aqueous solution (2:2: 1, v/v/v), vortexed, ultrasonicated at low temperature for 30 min, left to stand at −20 ℃ for 10 min, centrifuged at 14,000 × g and 4 ℃ for 20 min, and vacuum dried. Subsequently, 100 µL of acetonitrile solution was added during mass spectrometry (acetonitrile: Water = 1:1, v/v), redissolved, swirled, and centrifuged 14,000 × g and 4 ℃ for 15 min; the supernatant was collected for analysis. The samples were separated using an Vanquish LC ultra-high-performance liquid chromatography (UHPLC) HILIC column and analyzed using a Q Exactive HF-X mass spectrometer.

Partial least squares discriminant analysis (PLS-DA) [43] was performed using the *Ropls* package in R. The threshold for differential metabolites was determined using a variable importance in projection (VIP) > 1. The fold changes (FCs) and P-values of important metabolites

between the different treatments were calculated using the *edgeR* package. In the random forest model [44], the recursive feature elimination algorithm was employed for feature selection, and the classification errors were calculated to measure the importance of each metabolite in the random forest model. The results of VIP in PLS-DA and variable importance in the random forest were measured to determine the influence intensity and interpretation ability of each metabolite component on sample classification and discrimination and to assist metabolite filtering. Correlation analyses between key species and differential metabolites were performed using Spearman's algorithm.

The Kyoto Encyclopedia of Genes and Genomes (KEGG) database (https://www.genome.jp/kegg/pathway.html) is a powerful tool for in vivo metabolic analysis and network research. KEGG pathway enrichment analysis [45, 46] uses the KEGG pathway as a unit and the metabolic pathways of key species or closely related species as a background. Fisher's exact test was employed to calculate the significance level of metabolite enrichment in each pathway, thereby identifying significantly affected metabolic and signal transduction pathways. A smaller P-value indicates a more significant difference in the metabolic pathway.

Multi-omics joint analysis

The Procrustes analysis [47]—a method for comparing the consistency of microbial and metabolite data by analyzing the shape distribution—was performed. Additionally, multiple factor analysis (MFA)—an extension of principal component analysis (PCA) that describes the interrelationships among multiple sets of variables [48]—was employed. The distance between the objects was determined by synthesizing the contribution of each group of variable sets and balancing the influence of each group of variables. The object characteristics described by several groups of variables and the comprehensive relationships between the observed variables were analyzed. In the MIMOSA2 analysis [49], metabolic models of key microbial data were constructed using the reference database Refseq/EMBL_GEM, and their community metabolic potential (CMP) was calculated. Finally, pooled regression analyses were conducted to evaluate the predictive ability of key microbes for specific metabolites.

In addition, KEGG was employed to build a background database; an enrichment analysis network was established using the diffusion algorithm and normal approximation statistical methods in the FELLA package [50]. Subsequently, information on the important metabolites and metabolite-related intermediate substances (such as modules, enzymes, and reactions) participating in the relevant network was attained. Finally, based on the research of Yu et al. [51], the Metorigin toolbox (https://metorigin.met-bioinformatics.cn/home/) was applied to distinguish between microbial and host metabolites.

Statistical analysis

All statistical analyses were performed using GraphPad Prism software version 8 and IBM SPSS 26.0. Data were expressed as mean ± standard deviation (SD). The differences between the two groups were assessed by a two-tailed Student's *t*-test, and differences among three groups were evaluated by one-way analysis of variance followed by a post hoc least significant difference test. Nonparametric tests, including the Kruskal–Wallis test and Wilcoxon rank-sum test, were used to assess the 16S rRNA gene sequencing data of the three groups. Generally, a $P < 0.05$ was considered statistically significant.

Results

Lactobacillus Johnsonii YH1136 alleviates SCZ-like behavior in mice

Various behavioral tests were performed on the Ctrl, SCZ, and SCZ-P mouse groups (Fig. 1a). In the EPMT, compared with Ctrl mice, a significant difference was observed in the time spent in the open arms between the SCZ and SCZ-P mice; compared with the SCZ group, mice in the SCZ-P group showed an increasing trend; however, the difference was not significant (Fig. 1b). Compared with Ctrl mice, in the 10-min OFT test, the total distance traveled (Fig. 1c) and mean velocity traveled (Fig. 1d) of mice in the SCZ group were significantly increased, exhibiting obvious hyperactivity and repetitive behavior. In contrast, the performance of SCZ-P mice was significantly improved compared with Ctrl mice. In the sociability test (TCST test), the Ctrl and SCZ-P groups showed a significantly higher ratio of interaction time (around the wire cage with the strange mouse) than the SCZ mice (Fig. 1e), indicating improved sociability in SCZ-P mice. In the social novelty test (TCST test), the Ctrl and SCZ-P groups showed a significantly higher ratio of interaction time (around the wire cage with the novel strange mouse) than the SCZ mice (Fig. 1f), indicating improved preference for social novelty in SCZ-P mice.

Lactobacillus Johnsonii YH1136 intake affects the expression of tryptophan metabolism-related genes in the prefrontal lobe and hippocampus

The cortical mRNA expression of rate-limiting enzymes in the tryptophan metabolic pathway were compared between the Ctrl, SCZ, and SCZ-P groups. The SCZ group presented a significant decrease in *Bdnf* mRNA expression in the hippocampus compared with the other groups. However, in the PFC, while the SCZ group

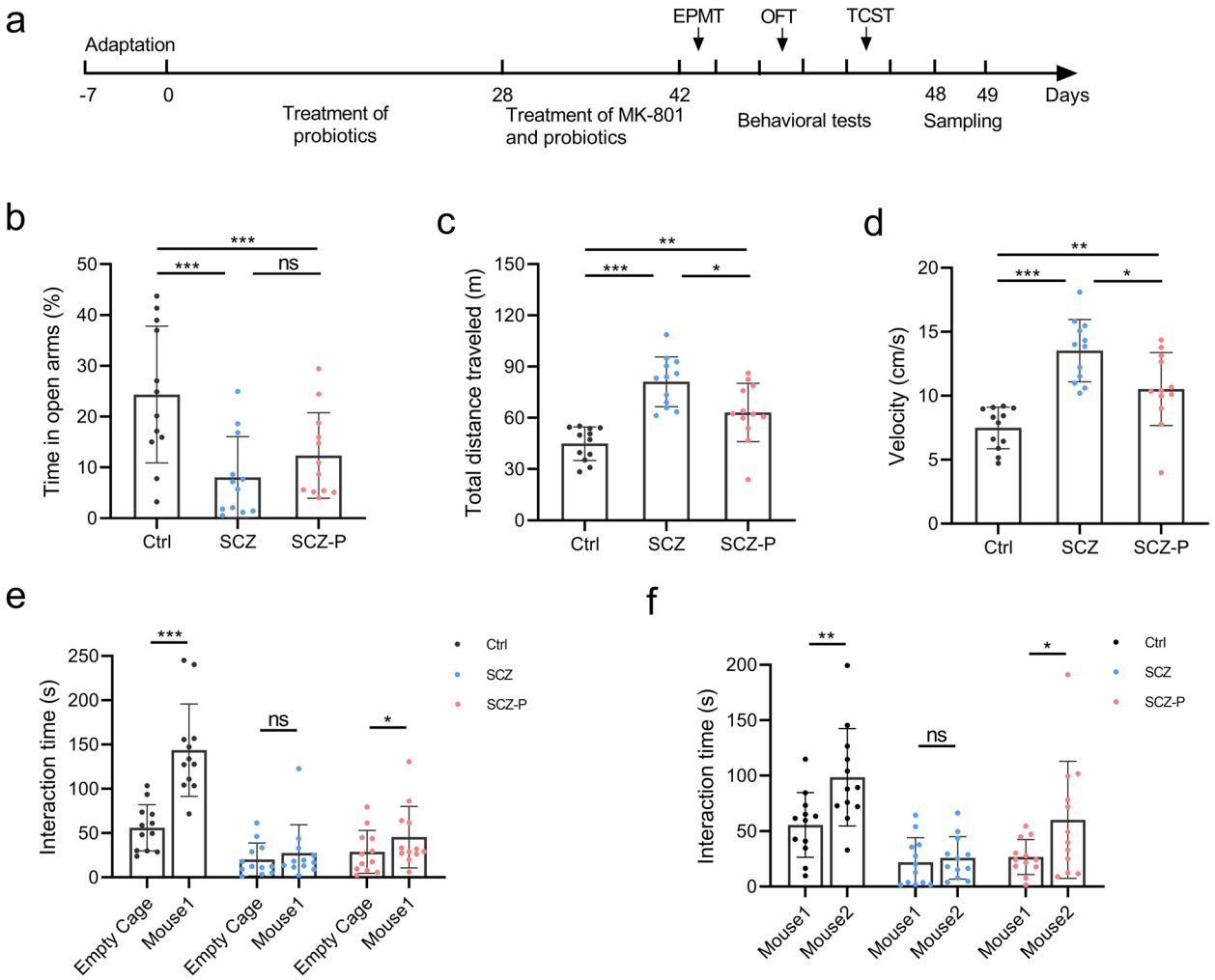

Fig. 1 The behavior performance in three group mice. **a** Experiment design. **b** Time in open arms of the elevated plus maze during 5-min exploration. **c** The cumulative distance (meters) traveled in the different zones, the representative traces of mouse activity. **d** The mean velocity traveled in the different zones. Sociability **(e)** and social novelty **(f)** of three groups in TCST. Means ± SD were presented in B-F and each circle represents individual mouse ($n = 12$ per group). ns no significant, $^{*}P < 0.05$, $^{**}P < 0.01$, $^{***}P < 0.001$

exhibited significantly decreased *Bdnf* mRNA expression compared with the Ctrl group, a non-significant decrease was observed compared with the SCZ-P group. The difference in *Bdnf* mRNA expression between the Ctrl and SCZ-P groups was significant in the PFC but not in hippocampus (Fig. 2a). Additionally, the SCZ group exhibited increased *Ido1, Kat1, Tph1,* and *Nr2b* mRNA transcription in the hippocampus and PFC, increased *Tdo2* expression in the hippocampus, and increased *Ido2* and *Kat3* expression in the PFC compared with the Ctrl and SCZ-P groups. Significant differences were not observed in *Kat2, Kat4, Nr1,* or *Nr2a* expression among the groups (Fig. 2b–2l).

To further verify the effect of *L. Johnsonii* YH1136 on tryptophan metabolism in the central nervous system, the abundances of TDO2, IDO1, IDO2, TPH1, and KAT1 proteins were evaluated via immunofluorescence staining. These results were consistent with mRNA expression (Fig. 3). The abundance of TDO2, IDO1, KAT1, and TPH1 increased within the hippocampus of SCZ mice; however, YH1136 intake significantly alleviated these effects. Meanwhile, IDO2 abundance was relatively high in the hippocampus and PFC across treatment groups, with YH1136 exerting a relatively weak effect.

Lactobacillus Johnsonii YH1136 intake alters the microbial diversity and composition in the ileum

In the ileum contents, 3,394,469 initial reads were generated from the MiSeq platform, and 1,670,854 clean reads were retained after filtering for low-quality reads.

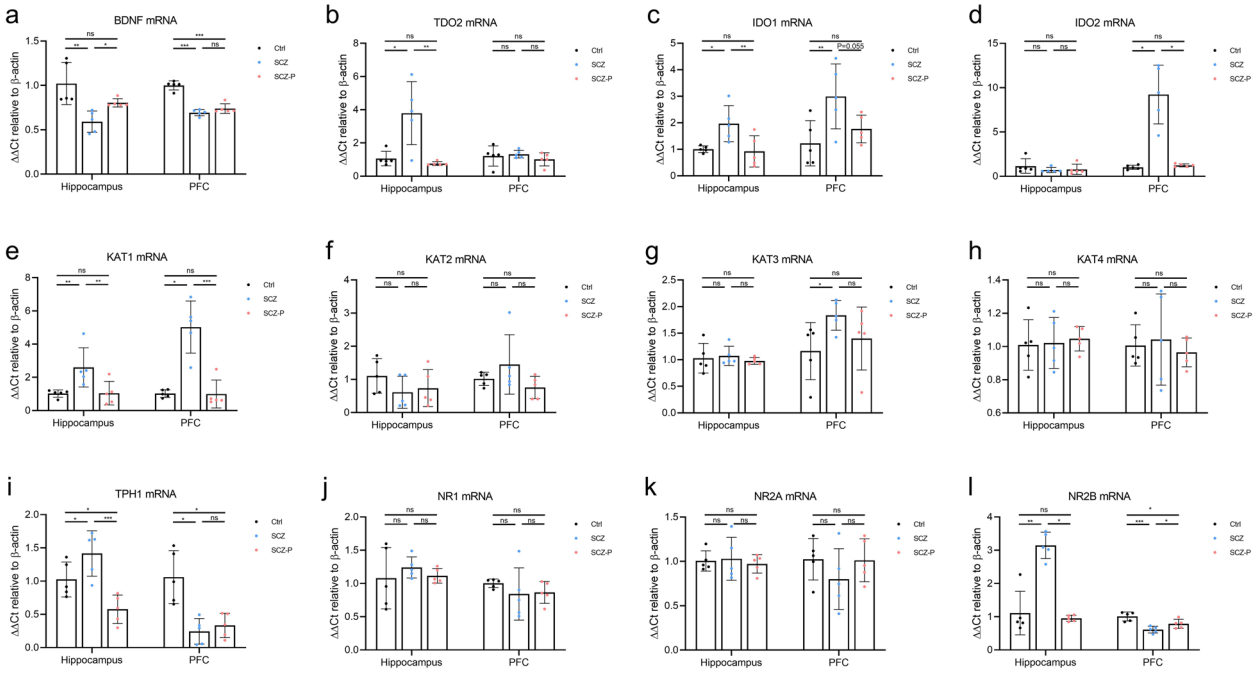

Fig. 2 The expression of related proteins in the hippocampus and prefrontal cortex (PFC) of mice. mRNA expression level of BDNF (**a**), TDO2 (**b**), IDO1 (**c**), IDO2 (**d**), KAT1 (**e**), KAT2 (**f**), KAT4 (**g**), KAT4 (**h**), TPH1 (**i**), NR1 (**j**), NR2A (**k**), and NR2B (**l**) in the Hippocampus and PFC. Data are expressed as mean ± SD (n = 5 per group). ns no significant, **P* < 0.05, ***P* < 0.01, ****P* < 0.001

The number of high-quality reads per sample was 69,619, ranging from 46,068 to 89,969 across all samples. A total of 2,143 features (ASVs) were identified.

A total of 3,385,542 initial reads were generated from the MiSeq platform for the colon samples, and 1,339,977 clean reads were retained after filtering for low-quality reads. There were 55,832 high-quality reads per sample, ranging from 43,427 to 70,757. In total, 4,032 features (ASVs) were identified. The sparse curve results indicated that all samples reached the platform level; hence, the sequencing depth met the requirements for further analysis.

The richness (Chao1 index) of the ileal microbiota was not significantly altered among the three groups (Fig. 4a). Compared with Ctrl mice, ileum microbiota diversity (Shannon diversity) decreased significantly in SCZ mice ($P < 0.05$); this reduction was improved by *L. Johnsonii* YH1136 treatment, although the improvements were not significant compared with the SCZ group ($P > 0.05$; Fig. 4b). Moreover, the structural differences among Ctrl, SCZ, and SCZ-P group samples were significant in PCoA analysis ($P < 0.05$), further highlighting the effect of supplementation with *L. Johnsonii* YH1136 on the ileum microbiota in SCZ mice (Fig. 4c).

Analysis of rich and rare taxa revealed that the AAT group accounted for a high proportion of ileal microbes in the Ctrl and SCZ groups, whereas the CAT and CART groups accounted for a relatively low proportion. Supplementation with *L. Johnsonii* YH1136 significantly increased the proportion of the CAT and CART groups while reducing that of the AAT group (Fig. 4d). At the phylum level, the most abundant taxa among all groups were Bacteroidetes, Firmicutes, and Actinobacteria (Fig. 4e). However, their absolute abundances varied between the treatments. Ten dominant genera were observed in all groups, with the top three identified as *uncultured bacterium*, *Lactobacillus*, *Dubosiella* (Fig. 4f). Compared with the Ctrl ($P < 0.05$) or SCZ group ($P < 0.05$), the relative abundance of *Lactobacillus* (Fig. 4g) significantly increased in SCZ-P mice, while the relative abundance of *Dubosiella* (Fig. 4h) significantly decreased ($P < 0.001$, $P < 0.01$, respectively).

However, these characteristics were not observed in the colon microbiota (Fig. 5a–c), with the alpha and beta diversity not differing significantly among the three groups ($P > 0.05$). In rich and rare taxa analysis, the proportion of each abundance group was similar among groups (Fig. 5d). This suggests that the therapeutic effect of *L. Johnsonii* YH1136 on SCZ may be related to improved microbial diversity and intestinal flora structure within the ileum. At the phylum level, the most abundant taxa among all groups were Bacteroidetes, Firmicutes, and Actinobacteria (Fig. 5e). Ten dominant genera were observed in all groups, with the top

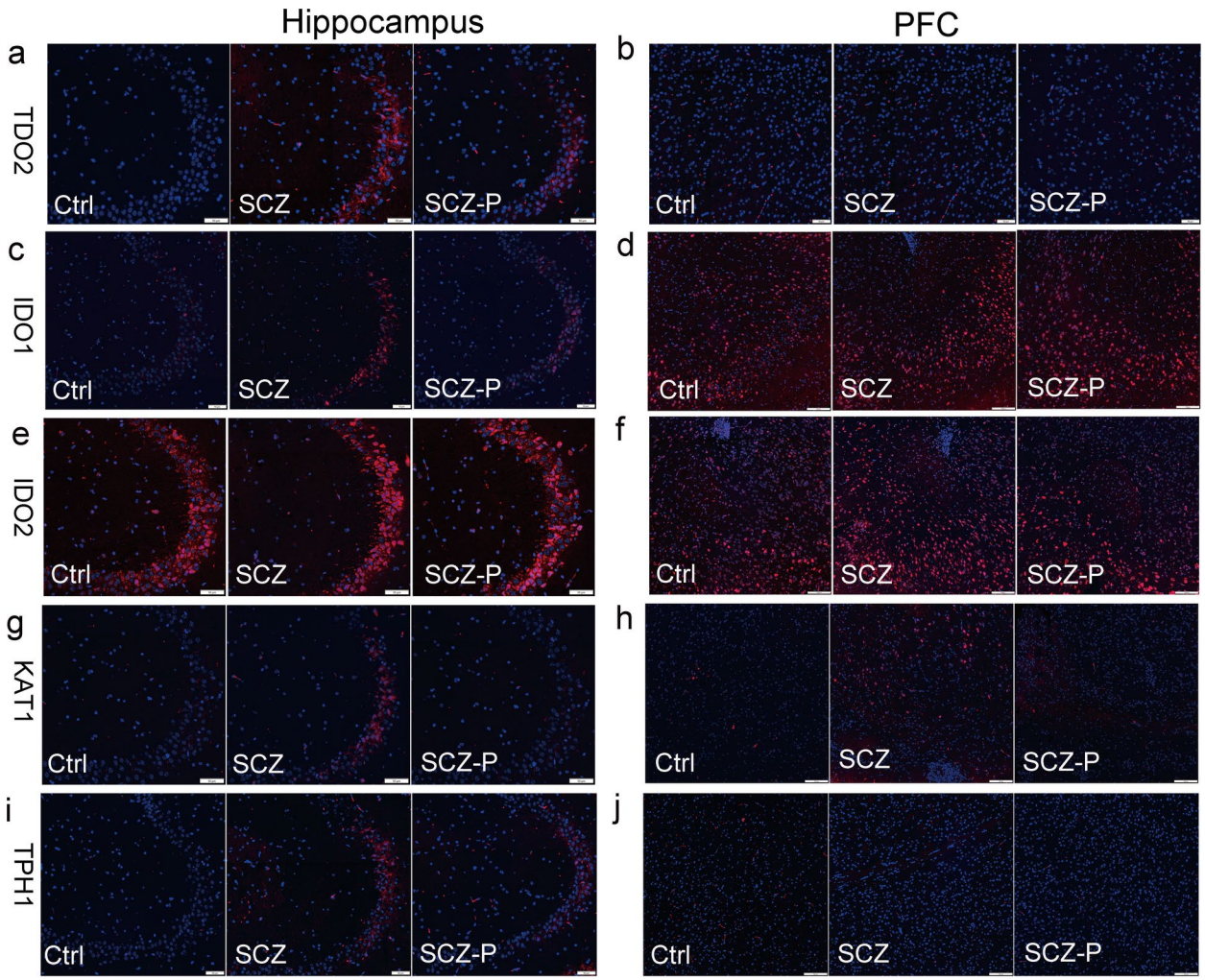

Fig. 3 Immunofluorescence staining. The sections of the TDO2 (**a**-**b**), IDO1 (**c**-**d**), IDO2 (**e**–**f**), KAT1 (**g**-**h**), TPH1 (**i**-**j**) in hippocampus and PFC. The magnification is 20X (F)

three identified as *uncultured bacterium*, *Lactobacillus*, *Dubosiella* (Fig. 5f).

Co-*occurrence* network and niche overlap analysis of key gut species in the ileum

According to the diversity index analysis, ileum microflora played a more significant role in ameliorating SCZ-like symptoms following *L. Johnsonii* YH1136 supplementation. Accordingly, indicator species and specificity-occupancy analyses were performed to identify key species in the ileum. The results showed shared indicator microbes within the ileum microflora of the Ctrl, SCZ, and SCZ-P groups. The indicator microbial species in the SCZ and SCZ-P groups were concentrated in Firmicutes. Meanwhile, Firmicutes and Bacteroidetes species were shared between the Ctrl and SCZ-P groups, and common Actinomycetes species were observed between the Ctrl and SCZ groups (Fig. 6a). The indicator ASVs (Table 2) included ASV52 (Muribaculaceae), ASV64 (*Lactobacillus*), ASV13 (*Dubosiella*), ASV76 (Muribaculaceae), ASV121 (Muribaculaceae), ASV132 (*Candidatus Saccharimonas*), ASV139 (*Turicibacter*), ASV146 (*Allobaculum*), ASV217 (Actinobacteria), ASV7 (*Lactobacillus*), ASV102 (Muribaculaceae), ASV180 (*Lachnospiraceae*). These indicator species were obtained based on their statistical significance ($P < 0.05$) and marked correlations between the ASV and one or more ASVs.

The SPEC-OCCU plot (Fig. 6b) shows the distribution and relative abundance of ASVs in the ileum gut flora of each group. The SCZ group had the largest number of specialists, including Firmicutes, Bacteroides, and Actinobacteria, while the Ctrl and SCZ-P groups had fewer and similar types of specialists, none of which included Actinobacteria (Table 2). This result further supports the indicator species results, suggesting that *L. Johnsonii* YH1136 supplementation may reduce the number

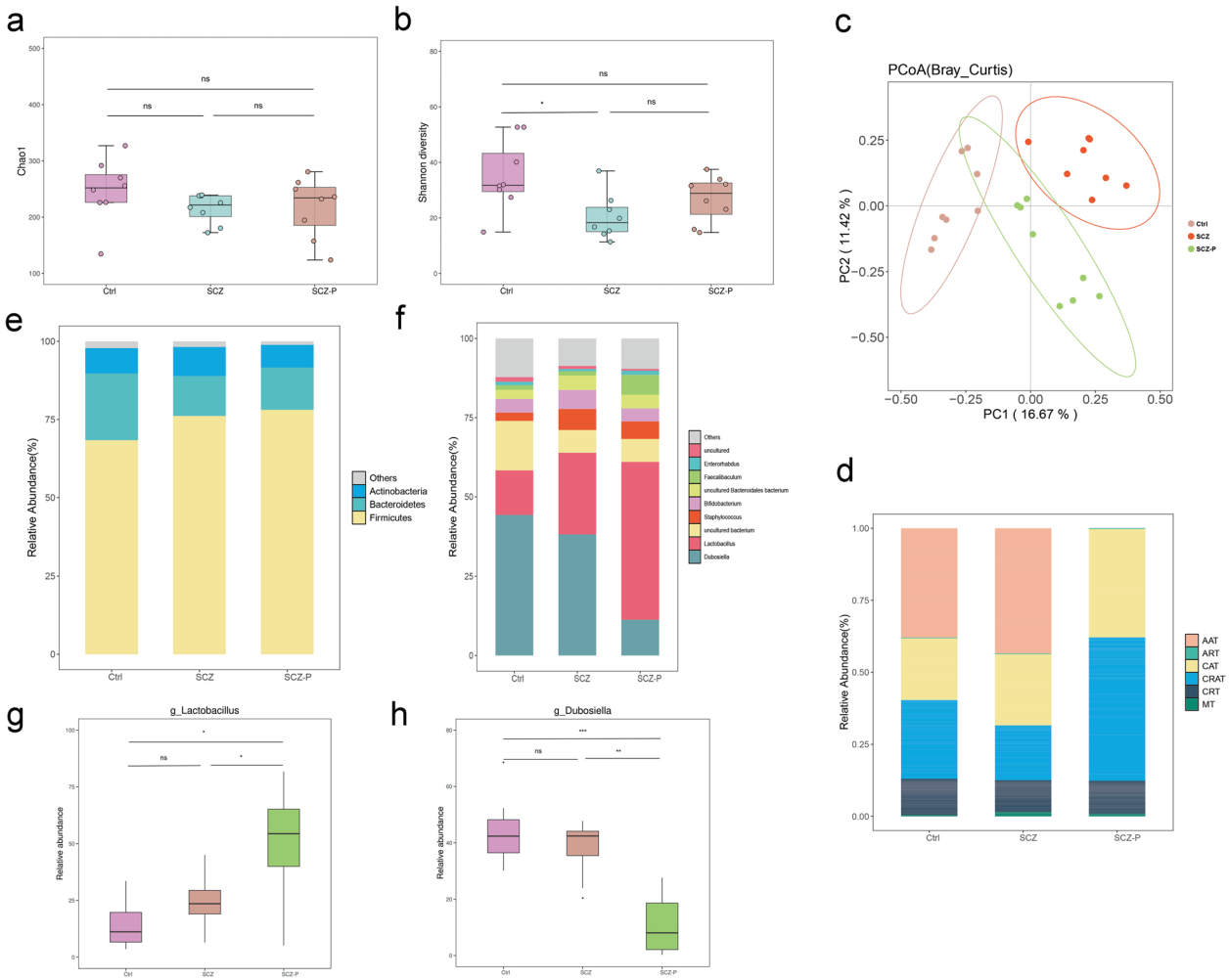

Fig. 4 Alpha, Beta diversity and microbial composition of ileum in mice. **a** Chao1 index. **b** Shannon diversity index. **c** Principal coordinate analysis (PCoA). **d** Rich and rare taxa analysis. Taxonomic distributions of bacteria at the (**e**) Phylum and (**f**) Genus. **g-h** The relative abundance of *Lactobacillus* and *Dubosiella*, respectively. All data are presented as mean ± SD ($n = 8$ per group). ns no significant, *$P < 0.05$, **$P < 0.01$, ***$P < 0.001$

of active Actinobacteria related to SCZ-like symptoms and increase the activity of Bacteroidetes, more closely resembling that of control mice performance.

Through MENA of the molecular ecological networks (MENs) of ileal microbes in the Ctrl (Fig. 6c), SCZ (Fig. 6d), and SCZ-P (Fig. 6e) groups, key microbial nodes were identified in each group of interacting networks (Table 3). In the Ctrl group, the node with max degree was ASV50 (Muribaculaceae), the node with max betweenness and max stress centrality was ASV60 (*Thermus*), and the node with max eigenvector centrality was ASV33 (*Lactobacillus*). In the SCZ group, the node with max degree, max betweenness, and max stress centrality was ASV23 (Muribaculaceae), while the node with max eigenvector centrality was ASV12 (*Dubosiella*). In the SCZ-P group, the node with max degree, max betweenness, max stress centrality, and max eigenvector centrality was ASV170 (Muribaculaceae).

According to the NOI results, the Ctrl (Fig. 6f), SCZ (Fig. 6g), and SCZ-P (Fig. 6h) contained the same key species, ASV102 (Muribaculaceae), of the SCZ-P group in the niche network. The niche overlap relationship among key species was weak in the Ctrl and SCZ-P groups, while the relationship among key species was obvious in the SCZ group. In addition, only the Ctrl group key species ASV64 (*Lactobacillus*), not ASV52 (Muribaculaceae), was present in the SCZ group. In contrast, only the Ctrl group key species ASV52 (Muribaculaceae), not ASV64 (*Lactobacillus*), were present in the SCZ-P group. These results suggest that Bacteroides is a key class of bacteria that affects the onset of SCZ-like symptoms and the intervention effect of *L. Johnsonii* YH1136.

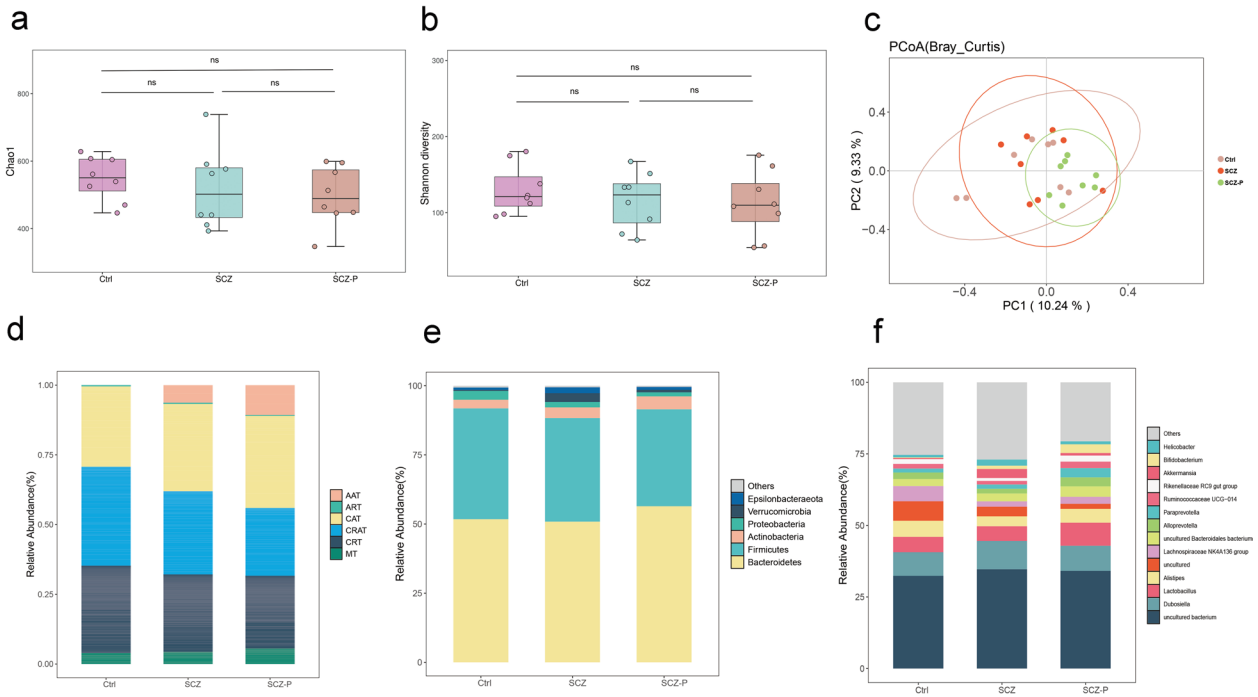

Fig.5 Alpha, Beta diversity and microbial composition of colon in mice. **a** Chao1 index. **b** Shannon diversity index. **c** Principal coordinate analysis (PCoA). **d** rich and rare taxa analysis. Taxonomic distributions of bacteria at the (**e**) Phylum and (**f**) Genus. All data are presented as mean ± SD ($n = 8$ per group). ns no significant

Subsequently, functional predictions of the differential flora were made based on the KEGG database by PICRUSt2 (Fig. 7). Compared with the Ctrl group, four pathways were significantly downregulated in the SCZ group: L-glutamate degradation V (via hydroxyglutarate), glutaryl-CoA degradation, sucrose degradation II (sucrose five metabolic pathways, synthase, glycogen degradation II (eukaryotic)), and L-arabinose degradation IV. Compared with the SCZ group, five pathways were significantly upregulated in the SCZ-P group, including isopropanol biosynthesis, phenylpropanoate and 3-(3-hydroxyphenyl) propanoate degradation to 2-oxopent-4-enoate, the super pathway of L-tryptophan biosynthesis, cinnamate and 3-hydroxycinnamate degradation to 2-oxopent-4-enoate, and sulfoglycolysis, while the glycolysis V (*Pyrococcus*) pathway was significantly downregulated.

Serum *metabolites* are altered following *Lactobacillus Johnsonii* YH1136 intake

Liquid chromatography-mass spectrometry was used to analyze the composition and changes in serum metabolites. In all serum samples, 922 metabolites were identified after combining the positive and negative ion modes, of which 435 and 487 metabolites were identified by the positive and negative ion modes, respectively. In the positive ion mode (Fig. 8a), lipids and lipid-like molecules, organic acids and derivatives, organoheterocyclic compounds, benzenoids, organic nitrogen compounds, organic oxygen compounds, phenylpropanoids and polyketides, nucleosides, nucleotides and analogs, and organosulfur compounds were detected in all samples. In the negative ion mode(Fig. 8b), lipids and lipid-like molecules, organic acids and derivatives, benzenoids, organic oxygen compounds, organoheterocyclic compounds, phenylpropanoids and polyketides, nucleosides, nucleotides, analogs, homogeneous non-metal compounds, lignans, neolignans and related compounds, and organic nitrogen compounds were detected.

To identify the serum metabolites that contributed the most to sample separation among the three groups, a PLS-DA model was established, and a score map was established based on the data obtained from the serum extracts in positive and negative ion modes. Given that samples in the same physiological and pathological states typically have similar metabolic compositions, they also appear in similar positions on the score map. The farther the relative positions between the samples, the greater the difference in physiological and pathological states between the samples. In the positive and negative ion modes, the metabolites were relatively close to each other among the samples of each group. However, a significant

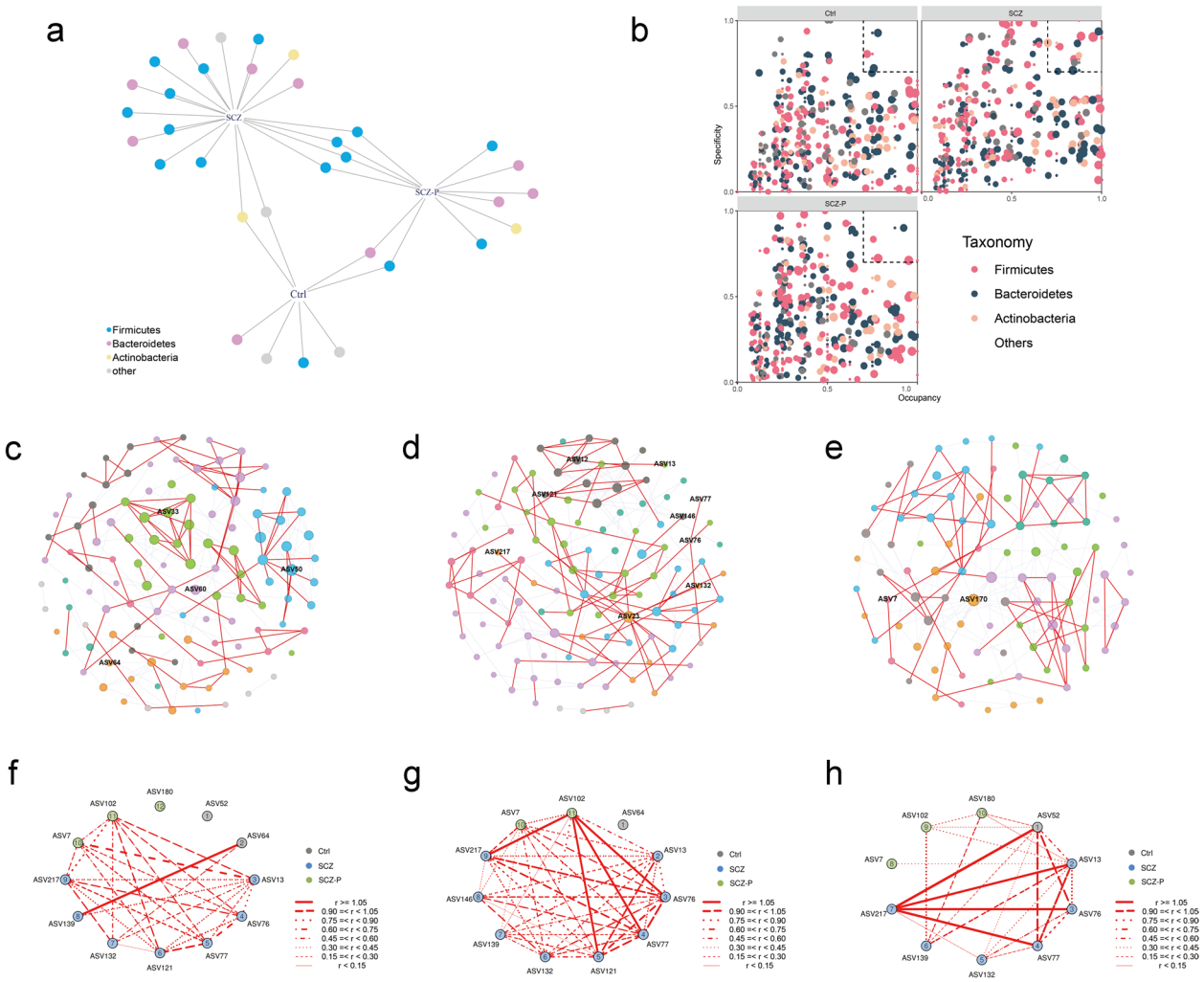

Fig. 6 The key species analysis of ileal microbiota. **a** Ileal microbial indicator species analysis. **b** Specifity and occupancy analysis. **c-e** MEN analysis results of Ctrl, SCZ, and SCZ-P groups, respectively. **f–h** NOI network diagram among key species in Ctrl, SCZ, and SCZ-P groups, respectively

separation was observed between the SCZ and Ctrl groups and between the SCZ and SCZ-P groups, whereas the Ctrl and SCZ-P groups were relatively close (Fig. 8c and d).

Subsequently, FC > 1.5 or FC < 0.5 and $P < 0.05$ were applied to identify metabolic biomarkers. Compared with the Ctrl group, under positive and negative ion modes, fewer metabolites were up-regulated and down-regulated in the SCZ group than in the SCZ-P group (Fig. 8e). To further evaluate the differences between metabolites in the different treatment groups, a random forest SCZ was established for classification prediction. The results showed the top 20 markers of difference between the SCZ and Ctrl groups (Fig. 8f) and between the SCZ and SCZ-P groups (Fig. 8g). Benzamide and Leonurine were significantly downregulated in the SCZ group (Fig. 8f); this effect was reversed by *L. Johnsonii* YH1136 (Fig. 8g). Ultimately, 43 major differential metabolites were screened; cluster analysis determined whether metabolites clustered together had similar expression patterns, similar functions, or participated in the same metabolic processes or cell pathways (Fig. S1).

Enrichment analysis of the KEGG pathways improved the efficiency of metabolite screening. The top 20 altered metabolic pathways were identified between the SCZ and Ctrl groups, SCZ-P and SCZ groups, and SCZ-P and Ctrl groups (Fig. 8h–j). Compared with the Ctrl group, the tryptophan metabolic pathway was upregulated in the SCZ group, whereas the SCZ-P group did not target this pathway among the top 20 ranked pathways. These changes not only reflect dysregulation of tryptophan metabolism in the SCZ group but also reveal the potential role of these metabolic pathways in SCZ. *L. johnsonii* YH1136 intake may

Table 2 The key species of three group with Spec-Occu analysis

Group	OTU	Specificity	Occupancy	Taxonomy
Ctrl	ASV43	0.721520142	0.75	Bacteroidetes
Ctrl	ASV52[a]	0.927766604	0.75	Bacteroidetes
Ctrl	ASV64[a]	0.804860824	0.75	Firmicutes
SCZ	ASV2	0.904167452	1	Firmicutes
SCZ	ASV13[a]	0.894902343	1	Firmicutes
SCZ	ASV21	0.709260273	0.875	Bacteroidetes
SCZ	ASV22	0.908757066	0.875	Firmicutes
SCZ	ASV42	0.869908306	0.75	Actinobacteria
SCZ	ASV65	0.774911646	0.875	Firmicutes
SCZ	ASV76[a]	0.926458837	1	Bacteroidetes
SCZ	ASV77[a]	0.936581675	1	Bacteroidetes
SCZ	ASV121[a]	0.866582669	0.875	Bacteroidetes
SCZ	ASV132[a]	0.754749144	0.875	Patescibacteria
SCZ	ASV139[a]	0.847411863	0.75	Firmicutes
SCZ	ASV146[a]	1	0.875	Firmicutes
SCZ	ASV162	0.703949702	0.75	Bacteroidetes
SCZ	ASV217[a]	0.796463592	0.875	Actinobacteria
SCZ-P	ASV7[a]	0.711059664	1	Firmicutes
SCZ-P	ASV10	0.722414425	0.75	Firmicutes
SCZ-P	ASV102[a]	0.900832604	0.875	Bacteroidetes
SCZ-P	ASV180[a]	0.834347877	0.75	Firmicutes

[a] The key species occurred in indicator species analysis

modulate these metabolic pathways through intestinal flora to ameliorate SCZ-like symptoms. The enrichment network was visually depicted using the aPEAR R package [52] and presented in Fig. S2.

Altered gut microbes in SCZ-P mice and their effect on behavioral and metabolic changes

A significant correlation was identified between ileal microbial populations and serum metabolites in the different groups ($M^2 = 0.76$, $P = 0.032$; Fig. 9a). This suggested that changes in serum metabolites caused by *L. johnsonii* YH1136 intake were related to changes in intestinal flora. Indeed, most of the intestinal flora were significantly correlated with changes in 42 metabolites (Fig. 9b). Therefore, M308T298 (KEGG ID: C19910, N-acetylneuraminic acid), a natural sugar acid present in organisms that normally acts as the end structure of the sugar chain and is involved in cell–cell recognition and signaling, was negatively correlated with ASV13 (*Dubosiella*) a key species in the SCZ group mice ($P < 0.05$).

The correlation and relative contribution between each variable set and the MFA axis were evaluated based on the position of the variable set in the ranking diagram (Fig. 9c). The coordinates of organoheterocyclic compounds and organic acids and derivatives on the first axis were relatively the same, meaning that their contributions to the first dimension were similar. For the second axis, lipids and lipid – like molecules and benzenoids had relatively large coordinates, indicating that they contributed the most to the second dimension.

The relationships between gut microbes and serum metabolites were explored based on the metabolic network method MIMOSA2. Well-predicted metabolites were identified by the CMP score model in all sample groups by a model using a local FDR q-value < 0.01 as

Table 3 Properties of three group MENs

Network Indexes	Ctrl (0.850)	SCZ (0.820)	SCZ-P (0.810)
Total nodes	115	116	92
Total links	225	193	181
Average degree (avgK)	3.913	3.328	3.935
Average clustering coefficient (avgCC)	0.276	0.167	0.175
Average path distance (GD)	5.408	4.781	4.36
Maximal degree	11	14	15
Centralization of degree (CD)	0.063	0.094	0.124
Maximal betweenness	2313.201	2477.209	910.637
Centralization of betweenness (CB)	0.331	0.352	0.187
Maximal stress centrality	32,233	11,120	3496
Centralization of stress centrality (CS)	4.67	1.55	0.701
Maximal eigenvector centrality	0.331	0.369	0.381
Centralization of eigenvector centrality (CE)	0.293	0.336	0.323
Density (D)	0.034	0.029	0.043
Reciprocity	1	1	1
Transitivity (Trans)	0.243	0.156	0.219
Connectedness (Con)	0.804	0.883	1

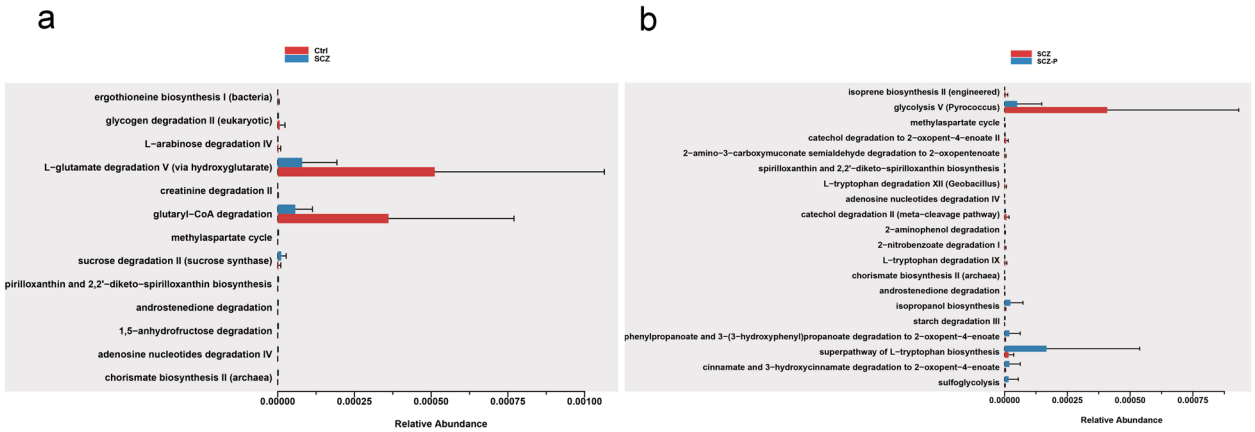

Fig. 7 The difference of KEGG enrichment analysis of ileal microbiota between Ctrl group and SCZ group (**a**) or between SCZ group and SCZ-P group (**b**)

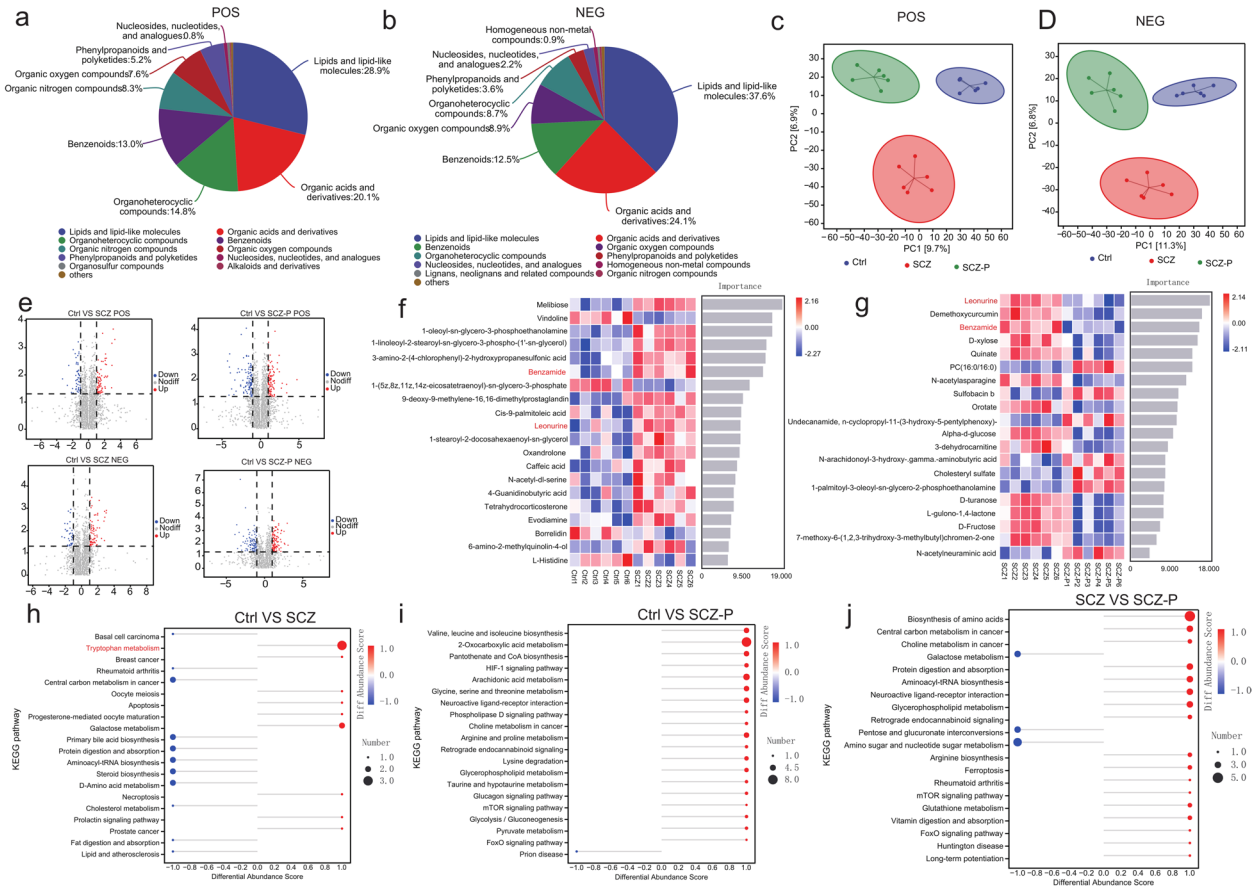

Fig. 8 The difference of metabolites in serum among Ctrl, SCZ and SCZ-P mice. **a**-**b** showed the identified serum metabolites in pos and neg ion modes, respectively. **c-d** established partial least squares discriminant analysis (PLS-DA) of metabolites in serum between the three groups in pos and neg ion modes, respectively. **(e)** Volcanic map shows different metabolites in serum among Ctrl, SCZ and SCZ-P mice. **f-g** Differentiated metabolites between groups (top20) selected according to feature importance, and the heat map shows the abundance distribution of these metabolites in each sample/group. **h-j** KEGG enrichment analysis of significantly altered metabolic pathways in serum among Ctrl, SCZ and SCZ-P mice. $n = 6$ per group

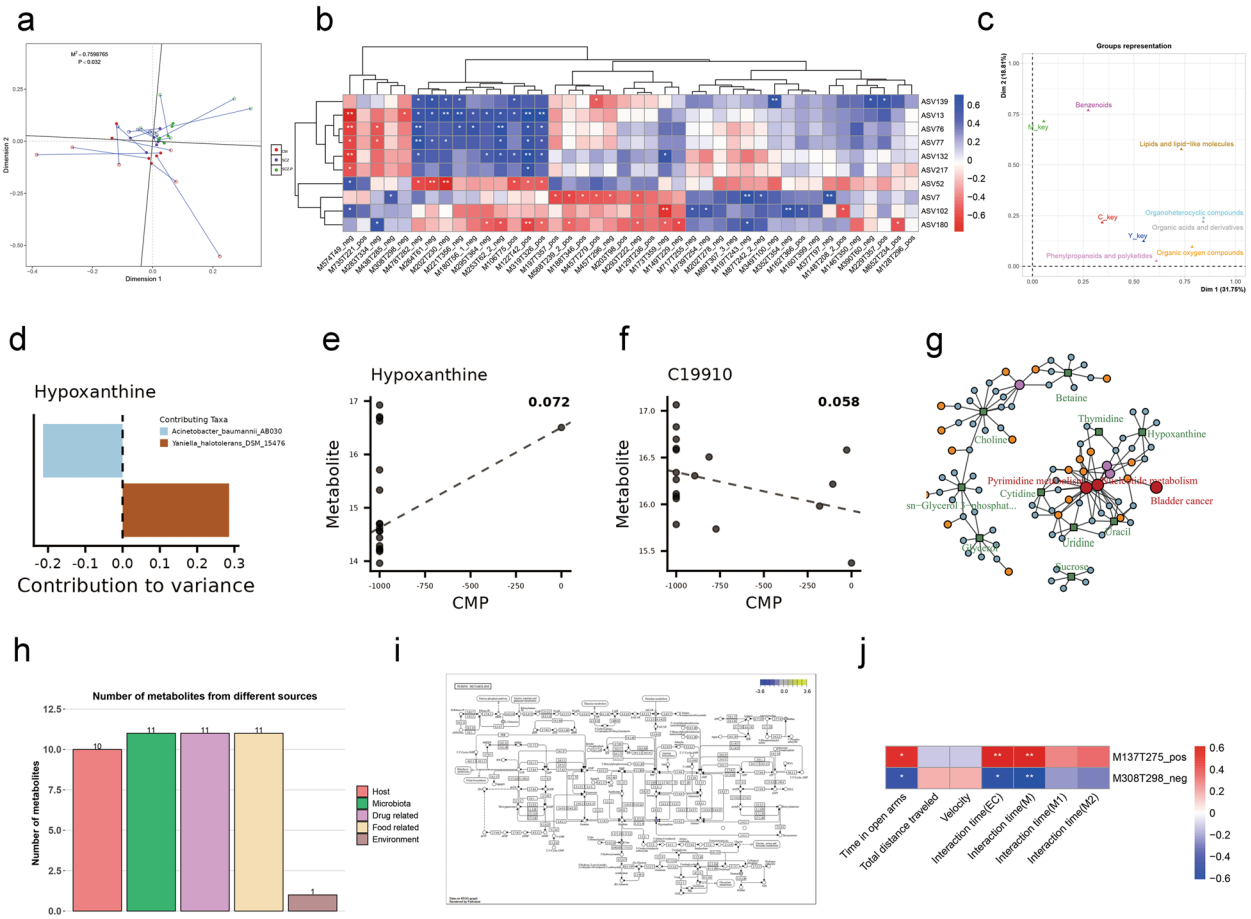

Fig. 9 Correlation analysis of different gut microbiota, metabolites and behaviors. **a** Procrustes analysis of serum metabolome and gut microbial. **b** Spearman correlation analysis of different gut microbiota and metabolites in serum. **c** Multivariate analysis of the relationship between the whole set of variables. **d** The contribution of taxa that explain the variation of the metabolite hypoxanthine; The dashed line to the left represents negative contributions and the dashed line to the right represents positive contributions. **e–f** The prediction of changes in key metabolite levels by community-level metabolic potential scores (CMP) is shown, respectively. **g** Diffusion analysis of differential metabolites in FELLA. **h** Map of differential metabolite quantities from different sources. **i** Visualization of nodes of the key metabolite hypoxanthine in the purine metabolic pathway. **j** Spearman correlation analysis of key metabolites and behavior performance. *$P < 0.05$, **$P < 0.01$

the significance threshold. Hypoxanthine (KEGG ID: C00262) was the only metabolite matched with a microbial contribution value < 0.1 and was affected by the production and consumption of *Lactobacillus animalis* KCTC 3501 DSM 20602 and *Lactobacillus intestinalis* DSM 6629 (Fig. 9d and e). In addition, the CMP value of N-acetylneuraminic acid (KEGG ID: C19910) was the second highest in the addition and regression of multiple samples, indicating that intestinal flora also exerted a certain ability to predict changes in N-acetylneuraminic acid (Fig. 9f). Interactive information on compounds, enzymes, reactions, modules, and pathways obtained through the FELLA package analysis showed that hypoxanthine was involved in pyrimidine metabolism, nutrient metabolism, and bladder cancer (Fig. 9g).

Using MetOrigin analysis, these important metabolites were grouped into five categories: 10 host (human)-derived metabolites, 11 bacteria-derived metabolites, and others belonging to drug, food, or environmental sources (Fig. 9h). Among these, the key metabolite C00262, hypoxanthine, had a host and microbial source, whereas C19910, N-acetylneuramic acid, had a microbial source. Furthermore, hypoxanthine was involved in the purine metabolic pathway and was at a pivotal position; it was significantly downregulated in the SCZ group compared with the Ctrl group (Fig. 9i).

Finally, Spearman's correlation coefficients between the two key metabolites and behavioral performance were calculated to further determine the role of these metabolites in the therapeutic effect of YH1136 in SCZ-like

behaviors. M308T298_neg (KEGG ID: C19910, N-acetylneuraminic acid) was significantly negatively correlated with open-arm activity time and social ability, whereas M137T275_pos (KEGG ID: C00262, hypoxanthine) was significantly and positively correlated with open-arm activity time and sociability (Fig. 9j).

Discussion

The recent development of psychobiotics has led to new solutions for the prevention and treatment of SCZ. Similar with previous preventive studies (such as, Mañé et al. administered probiotic or vehicle for 2 weeks before colitis [53]), in the present study, we supplemented probiotics before the disease modeling begins to achieve the preventive effect against disease onset and simulate a real probiotic usage environment. Collectively, behavioral experiments, 16S rRNA sequencing, serum metabolomics, and other omics analyses were performed to determine whether *L. Johnsonii* YH1136 ingestion via gavage effectively prevented SCZ-like behavior in mice and identify key species and metabolites that mediate the associated pathway.

Hyperactivity and repetitive movements are typical of MK-801-induced SCZ in mice and are consistent with positive symptoms in patients with SCZ [54]. Compared with Ctrl mice, the movement distance and speed of the SCZ group significantly increased in the open field test, consistent with a previous study [55]. In contrast, the performance of the SCZ-P group was relatively controlled with reduced psychomotor hyperactivity. Impairments in social ability and social novelty in the SCZ mice mirrored the impairments in cognitive function and social interaction in patients with SCZ, whereas the social ability and social novelty performance of the mice receiving YH1136 resembled those of the Ctrl group. This suggests that *L. johnsonii* YH1136 intake reduced the onset of negative SCZ-like behavior. Although significant differences were not observed between the SCZ and SCZ-P groups in the proportion of time spent in the open arm, an increasing trend was detected. This is similar with the results reported by Akosman et al. [25], who treated SCZ mice with resveratrol. These behavioral manifestations suggest that *L. Johnsonii* YH1136 can partially prevent SCZ-like behaviors.

The hippocampus and PFC are important for SCZ onset and development [55]. The PFC is closely related to cognition, working memory, and decision-making functions [56], whereas hippocampal lesions lead to impaired spontaneous alternation behavior [57]. Neurotrophic factors, including BDNF, are highly expressed in the hippocampus and PFC and promote neuronal development, maintain neuronal survival and function, and affect memory and cognition [58]. Antipsychotics increase plasma BDNF levels [59] and *Radix Bupleuri* aqueous extract upregulates BDNF levels in the hippocampus of SCZ mice [60]. In this study, the expression of BDNF was significantly reduced in the SCZ group, while *L. johnsonii* YH1136 intake upregulated its expression in the hippocampus of SCZ mice, demonstrating a neuroprotective role. Additionally, the low function of NR contributes to SCZ pathogenesis. NR is composed of subunits NR1, NR2 and NR3, NR1 is the essential subunit; NR2 has four different structures, NR2A, NR2B, NR2C and NR2D, among which NR2A and NR2B play a major role [61]. Similar to the current study results, Jia et al. [61] reported that the expression levels of NR1, NR2A, and NR2B did not differ significantly in the PFC of adult SCZ rats. Meanwhile, the expression levels of NR1 and NR2A significantly increased in the hippocampus. In the current study, the mRNA expression levels of *Nr1* and *Nr2a* in the hippocampus and PFC did not differ significantly among the three groups of mice. The upregulated *Nr2b* mRNA expression in the hippocampus of SCZ mice may be related to SCZ-positive symptoms, such as cognitive impairment [62], while the intake of *L. Johnsonii* YH1136 was resistant to this increase. Moreover, while *Tdo2, Ido1*, and *Ido2* expression were significantly increased in SCZ mice, this was reversed by supplementation with YH1136. These rate-limiting enzymes are involved in converting tryptophan to kynurenine in vivo. Hence, their upregulation indicates an imbalance in the kynurenine pathway during tryptophan metabolism, which is considered an important hypothesis in SCZ [63].

Zhu et al. reported that the kynurenine–kynurenic acid pathway of tryptophan catabolism is significantly enhanced in SCZ mice, while the serotonin pathway of tryptophan catabolism is significantly weakened [27]. During this process, the expression levels of transferases, such as KAT1–4, which convert kynurenine to kynurenic acid, become increased. Similarly, in the current study, the expression levels of *Kat1* and *Kat3* were significantly increased in mice in the SCZ group and lower in the SCZ-P group. These results suggest that ingesting *L. johnsonii* YH1136 effectively reduces SCZ-like symptoms and is associated with inhibiting overactivation of the tryptophane–kynurenine–kynuuric acid metabolic pathway.

Correlations have been identified between the central nervous system and the gut in terms of nutrition, immunology, neurotransmission, and endocrine signaling; it has been postulated that the gut microbiota can affect the body's immune and nerve functions [2]. Among them, disturbance of the intestinal microbiota may partly explain the heterogeneity of SCZ patients, altering the concentrations of intestinal metabolites and intestinal barrier function while promoting inflammatory

responses and oxidative stress [64]. In our previous study, fecal transplantation from patients with SCZ after treatment improved behavior and social ability in mice, revealing the causal relationship between gut microbiota and SCZ development [65].

Although probiotics have been widely used for treating neuropsychiatric diseases, current research lacks direct evidence that beneficial microbes in the gut can improve SCZ symptoms [66]. Additionally, studies have sought to characterize the microbiota composition and metabolites in patients with SCZ [15, 67]. For example, Wang et al. reported a significant association between differential metabolites and intestinal microbial species, confirming the role of *Bifidobacterium longum* gadB/gadC genes in gamma-aminobutyric acid (GABA) production, which may be the driving species in patients with SCZ [68]. In the current study, no differences were observed in the α-diversity indexes of the microbiota among the groups; however, the β-diversity differed. Li et al. [69] also noted that the evenness and richness of the intestinal flora in patients with SCZ did not differ significantly from those in the normal control group. In contrast, significant community-level separation occurred based on Bray–Curtis dissimilarity beta diversity. Additionally, the species composition in the ileum of SCZ and SCZ-P mice and the level of bacterial separation between groups was more obvious than in the colon. Additionally, many high-abundance microbial groups appeared in the ileum, implying that the ileum was more vulnerable to SCZ and probiotics. Specifically, the abundance of *Lactobacillus* spp. in the ileum of mice in the SCZ and SCZ-P groups gradually increased, whereas that of *Dubosiella* spp. gradually decreased across all three groups, suggesting that these two taxa may play different roles. Firstly, a significant increase in *Lactobacillus* spp. abundance was observed in the probiotic treatment group (SCZ-P group), which is likely attributable to the probiotic supplementation. Secondly, although previous studies have demonstrated an increased relative abundance of *Lactobacillus* spp. in the gut microbiota of SCZ patients, with this elevation being associated with more severe disease symptoms [70], the precise mechanism underlying this increase remains unclear. Notably, despite these uncertainties, *Lactobacillus* has been identified as a potential key regulator in SCZ pathogenesis. Based on prior evidence supporting the beneficial properties of strain *Lactobacillus Johnsonii* YH1136 [5, 18], we used it as treatment. In this study, we propose two potential explanations for the upward trend of *Lactobacillus* in the SCZ group: (1) it may represent a compensatory response to resist the effects of SCZ with some beneficial *Lactobacillus* spp. are elevated. In a randomized and double-blind study, Ghaderi et al. found that probiotic (mixture of *Lactobacillus reuteri*, *Lactobacillus fermentum*, *Lactobacillus acidophilus*, and *Bifidobacterium bifidum*) and vitamin D for 12 weeks to chronic schizophrenia had beneficial effects on the general and total PANSS score, and metabolic profiles [71]; (2) it could involve *Lactobacillus* strains with conditional pathogenicity, where specific pathogenic interactions might contribute to the observed phenomenon. The role of several strains of Lactobacillus in autoimmune diseases and other chronic diseases has been reviewed, and while these strains, such as *L. reuteri*, have been shown to provide immune health benefits, they have also been shown to act as pathogens in hosts prone to autoimmunity [72]. Collectively, these findings suggest that the increased *Lactobacillus* abundance in the SCZ-P and SCZ groups arises from distinct triggers. *Dubosiella* spp. are commonly infectious bacterial species; their enrichment may affect the occurrence of Alzheimer's disease in mice through palmitoleic acid in the cortex. All the above studies could prove that the occurrence and development of SCZ may be related to probiotics in the small intestine, especially in the ileum.

This study concurrently constructed the MENs of diverse microbial communities in the gut. Within each co-occurrence network of microbial communities, species with a high degree of betweenness centrality were identified as foundational species with a pivotal role in upholding the ecological framework and performing key ecological functions. Their absence would result in the breakdown of the entire network [73]. Various hub nodes on co-occurrence networks corresponding to "foundational species" serve as promising intervention targets [73, 74]. Further analysis revealed that the foundational species lacked specificity for various microbial environments. Consequently, based on variations in treatment methods, species that exhibit significant positive responses to distinct environments or ecological processes (Indicator species) were identified [75] and categorized as "environmental key response species" or "key species," characterized by high specificity and high occupancy rates within the gut microbiota [39]. Subsequent screening of key responsive species present in the Ctrl, SCZ, and SCZ-P group microecological environments identified *Dubosiella* (ASV13), *Candidatus Saccharimonas* (ASV132), and *Turicibacter* (ASV139) as key responsive species associated with SCZ-like symptoms in mice, while a key responsive *Lactobacillus* (ASV7) was found in SCZ-P mice. Key responsive species can adapt to changes in diverse microecological environments and are considered controllable within foundational species [76].

Serum metabolomic analysis identified major differential metabolites among treatment groups from the perspectives of PLS-DA and random forest. Unlike PCA,

which was used to observe the overall change trend, PLS-DA screened the differential metabolites between groups. In metabolomic analyses, PLS-DA can distinguish metabolites with the largest differential contribution between groups based on VIP values [77]. Similarly, as an integrated learning method, random forest can screen landmark metabolites by building multiple decision trees to solve classification and regression problems [78]. The differential metabolites identified in the serum were organoheterocyclic compounds, organic acids and derivatives, organic oxygen compounds, lipids and lipid-like molecules, phenylpropanoids, polyketides, and benzenoids. The degree of correlation among them differs and association analysis with key responsive species also shows that most of the metabolite changes may have a potential relationship with species that adapt to different ecological environments. Therefore, the intake of *L. johnsonii* YH1136 can profoundly affect the state of large number of metabolites in the blood, and preliminary reveal that these changes in metabolites have a certain potential relationship with intestinal key microorganisms.

Subsequently, the relationship between the key gut-responsive microbiota and serum metabolites were explored using the MIMOSA2 tool [49]. The metabolite hypoxanthine (KEGG ID: C00262) was identified as the only metabolite with a microbial contribution value < 0.1, which was affected by the generation and consumption of *Lactobacillus animalis* KCTC 3501 DSM 20602 and *Lactobacillus intestinalis* DSM 6629 species. In addition to hypoxanthine, the R^2 value in the CMP value sum regression of multiple N-acetylneuraminic acid (KEGG ID: C19910) samples was the highest, indicating that the intestinal flora also has a certain predictive ability for changes in N-acetylneuraminic acid. Meanwhile, the MFA analysis of the current study revealed that hypoxanthine and N-acetylneuraminic acid are organoheterocyclic compounds and organic oxygen compounds, respectively; their metabolite variable sets contributed significantly to the first-dimensional coordinate axis, indicating that the metabolites of these categories played an important role in the spatial ordering of samples. Similarly, Jin et al. reported a relationship between cellular purine anabolic dysfunction and chronic stress-induced psychological diseases. Specifically, excessive purines (hypoxanthine and xanthine) enter the brain through blood circulation, causing oligodendrocyte activation and proliferation, followed by neuronal overactivation in the left amygdala region, resulting in anxiety symptoms [68]. Another study reported that among the differential metabolites related to brain tissue injury, hypoxanthine positively correlated with GABA, dopamine, endorphin, IL-6, and TNF-α [79]. The stable synaptic link of nerve cells is the structural basis of memory formation, and N-acetylneuraminic acid is the nutrient of nerve cell membranes and synapses, which could promote the differentiation, development, and regeneration of nerve cells [80]. N-Aacetylneuraminic acid may play an important role in psychiatric diseases, a study reported that repeated administration of N-acetylneuraminic acid induces immune rearrangements associated with cognitive decline [81]. These results indicate that hypoxanthine and N-acetylneuraminic acid may play a key role in SCZ.

Subsequently, enrichment and network analyses were combined to explain the biological background of the affected metabolites. Meaningful subnetworks (diffusion) can identify key nodes in the network, including metabolite-related pathways, intermediate objects connecting metabolites, and metabolic pathways, such as modules, enzymes, and reactions [50]. Finally, using the manually validated metabolite database, the sources of metabolites affected by the microbiota were determined. The metabolite N-acetylneuraminic acid was determined to have been only produced by intestinal microbes and was regarded as a direct marker of microbial community activity. The other ten metabolites in meaningful subnetworks, such as hypoxanthine, were identified as metabolites co-metabolized by the host and gut microbes and may have bridging roles in microbe–host interactions. Among them, hypoxanthine was primarily enriched in the "mmu00230" pathway, related to purine metabolism in mice. Cui et al. demonstrated that purine and pyrimidine metabolism disordered in the SCZ prodromal period (clinical high risk, CHR). In the purine metabolic pathway, glycine, uric acid, and urate free radicals increase, whereas riboflavin decreases in the CHR and first-episode schizophrenia groups [82]. More specific pathways, such as metabolic nodes, are related to hypoxanthine like NAD + oxidoreductase and oxygen oxidoreductase reactions. Compared with the traditional enrichment analysis, the network analysis of metabolic pathways revealed that the enzymes of metabolite hypoxanthine-related reactions include purine nucleotide phosphorylase and thymidine phosphorylase, as well as modules of related reactions such as adenine ribonucleotide biosynthesis and guanine ribonucleotide biosynthesis, this results further reveal the role of hypoxanthine. Finally, the key metabolites, hypoxanthine and N-acetylneuraminic acid, obtained through the joint screening of the microbiome and metabolome data were significantly correlated with open-arm activity time ratio and sociability. These results indicate that the key metabolites mediate the regulation of anxiety and social behavior related to SCZ.

Conclusion

The findings of this study suggest that *L. Johnsonii* YH1136 supplementation via gavage mitigated SCZ-like behavior and modulated abnormal enzyme expression in SCZ mice. The compositional changes in ileal microbiota may play a significant role in the mechanism by which *L. johnsonii* YH1136 impacts SCZ, particularly in the relative abundance of *Lactobacillus* and *Dubosiella* genera. However, 16S rRNA sequencing provides taxonomic profiling but cannot fully characterize microbial functional interactions. Future studies need to further reveal through metagenomics how *L. johnsonii* YH1136 interacts with the original flora after entering the ileum. Furthermore, serum metabolites, particularly N-acetylneuraminic acid and hypoxanthine, may mediate the interaction between the MGBA and SCZ following *L. johnsonii* YH1136 ingestion as a psychobiotic. These preclinical findings provide basic theoretical support for the future development of probiotic formulations of *L. johnsonii* to help ameliorate symptoms of SCZ, including investigations into strain-specific effects and optimal dosing regimens.

Abbreviations

Actb	β-Actin
ASV	Amplicon sequence variant
AT	Abundant taxa
BDNF	Brain-derived neurotrophic factor
CAT	Conditionally abundant taxa
CFU	Colony forming units
CHR	Clinical high risk
CMP	Community metabolic potential
CRAT	Conditionally rare or abundant taxa
CRT	Conditionally rare taxa
Ctrl	Control
EPMT	Elevated plus maze test
FC	Fold change
GABA	Gamma-aminobutyric acid
IDO	Indoleamine-pyrrole 2,3-dioxygenase
IL	Interleukin
KAT	Kynurenine aminotransferase
KEGG	Kyoto Encyclopedia of Genes and Genomes
MEN	Molecular ecological network
MENA	Molecular ecological network analysis
MFA	Multiple factor analysis
MGBA	Microbiota–gut–brain axis
MRS	De Man, Rogosa, and Sharpe
MT	Moderate taxa
NOI	Niche overlap index
NR	N-methyl-D-aspartate receptor
OFT	Open field test
PANSS	Positive and negative Syndrome Scale
PBS	Phosphate-buffered saline
PCA	Principal component analysis
PCoA	Principal coordinate analysis
PFC	Prefrontal cortex
PLS-DA	Partial least squares discriminant analysis
RT	Rare taxa
RT-qPCR	Real-time quantitative PCR
SCZ	Schizophrenia
SD	Standard deviation
SPEC-OCCU	Specificity and occupancy
TCST	Three-chamber sociability test
TDO2	Tryptophan 2,3-dioxygenase
TNF	Tumor necrosis factor
TPH1	Tryptophan hydroxylase 1
UHPLC	Ultra-high-performance liquid chromatography
VIP	Variable importance in projection

Supplementary Information

The online version contains supplementary material available at https://doi.org/10.1186/s12866-025-03893-w.

Supplementary Material 1.

Authors' contributions

MX, XN, HL and TZ managed project and data. LZ, NS, JX, XG, BG and SB conducted experiments. LZ, NS and JX analyzed and interpreted the results. LZ, JX, HY prepared manuscript draft. LZ, HW and TZ revised and edited the manuscript. All authors read and approved the final manuscript.

Funding

The present study was supported by the Science and Technology Innovation 2030-Brain Science and Brain-Inspired Artificial Intelligence Key Project under Grant 2022ZD0208506, and the Sichuan Science and Technology Program (2024NSFSC0611, MZGC20230063,2025ZNSFSC0780).

Data availability

The data of 16S rRNA sequencing reads have uploaded to the National Center for Biotechnology Information (NCBI) BioProject database: PRJNA1172328. The database of the metabolomics URL: https://www.ebi.ac.uk/metabolights/MTBLS11385.

Declarations

Ethics approval and consent to participate

All animal experiment procedures were approved by the Institutional Animal Care and Use Committee of the Sichuan Agricultural University (approval number: SYXKchuan2019-187).

Consent for publication

Not applicable.

Competing Interests

The authors declare no competing interests.

Received: 29 October 2024 Accepted: 14 March 2025
Published online: 02 April 2025

References

1. Binda S, Tremblay A, Iqbal UH, Kassem O, Le Barz M, Thomas V, Bronner S, Perrot T, Ismail N, Parker JA. Psychobiotics and the Microbiota-Gut-Brain Axis: Where Do We Go from Here? Microorganisms. 2024;12(4):634. https://doi.org/10.3390/microorganisms12040634.
2. Wang HX, Wang YP. Gut Microbiota-brain Axis Chinese medical journal. 2016;129(19):2373–80. https://doi.org/10.4103/0366-6999.190667.
3. You M, Chen N, Yang Y, Cheng L, He H, Cai Y, Liu Y, Liu H, Hong G. The gut microbiota-brain axis in neurological disorders. MedComm. 2024;5(8):e656. https://doi.org/10.1002/mco2.656.
4. Socała K, Doboszewska U, Szopa A, Serefko A, Włodarczyk M, Zielińska A, Poleszak E, Fichna J, Wlaź P. The role of microbiota-gut-brain axis in neuropsychiatric and neurological disorders. Pharmacol Res. 2021;172:105840. https://doi.org/10.1016/j.phrs.2021.105840.
5. Zhang X, Jiang J, Xin J, Sun N, Zhao Z, Gan B, Jiang Y, Gong X, Li H, Ma H, Ni X, Chen Y, Bai Y, Wang H. Preventive effect of Lactobacillus johnsonii YH1136 against uric acid accumulation and renal damages. Front Microbiol. 2024;15:1364857. https://doi.org/10.3389/fmicb.2024.1364857.

6. Makki K, Deehan EC, Walter J, Bäckhed F. The Impact of Dietary Fiber on Gut Microbiota in Host Health and Disease. Cell Host Microbe. 2018;23(6):705–15. https://doi.org/10.1016/j.chom.2018.05.012.
7. Ashique S, Mohanto S, Ahmed MG, Mishra N, Garg A, Chellappan DK, Omara T, Iqbal S, Kahwa I. Gut-brain axis: A cutting-edge approach to target neurological disorders and potential synbiotic application. Heliyon. 2024;10(13): e34092. https://doi.org/10.1016/j.heliyon.2024.e34092.
8. Dinan TG, Stanton C, Cryan JF. Psychobiotics: a novel class of psychotropic. Biol Psychiat. 2013;74(10):720–6. https://doi.org/10.1016/j.biopsych.2013.05.001.
9. Luang-In V, Katisart T, Konsue A, Nudmamud-Thanoi S, Narbad A, Saengha W, Wangkahart E, Pumriw S, Samappito W, Ma NL. Psychobiotic Effects of Multi-Strain Probiotics Originated from Thai Fermented Foods in a Rat Model. Food science of animal resources. 2020;40(6):1014–32. https://doi.org/10.5851/kosfa.2020.e72.
10. Kahn RS, Sommer IE, Murray RM, Meyer-Lindenberg A, Weinberger DR, Cannon TD, O'Donovan M, Correll CU, Kane JM, van Os J, Insel TR. Schizophrenia Nature reviews Disease primers. 2015;1:15067. https://doi.org/10.1038/nrdp.2015.67.
11. Cacabelos R, Martínez-Bouza R. Genomics and pharmacogenomics of schizophrenia. CNS Neurosci Ther. 2011;17(5):541–65. https://doi.org/10.1111/j.1755-5949.2010.00187.x.
12. Gillespie AL, Samanaite R, Mill J, Egerton A, MacCabe JH. Is treatment-resistant schizophrenia categorically distinct from treatment-responsive schizophrenia? a systematic review. BMC Psychiatry. 2017;17(1):12. https://doi.org/10.1186/s12888-016-1177-y.
13. Shah P, Iwata Y, Plitman E, Brown EE, Caravaggio F, Kim J, Nakajima S, Hahn M, Remington G, Gerretsen P, Graff-Guerrero A. The impact of delay in clozapine initiation on treatment outcomes in patients with treatment-resistant schizophrenia: A systematic review. Psychiatry Res. 2018;268:114–22. https://doi.org/10.1016/j.psychres.2018.06.070.
14. Thirion, F., Speyer, H., Hansen, T. H., Nielsen, T., Fan, Y., Le Chatelier, E., Fromentin, S., Berland, M., Plaza Oñate, F., Pons, N., Galleron, N., Levenez, F., Markó, L., Birkner, T., Jørgensen, T., Forslund, S. K., Vestergaard, H., Hansen, T., Nordentoft, M., Mors, O., Ehrlich, S. D. Alteration of Gut Microbiome in Patients With Schizophrenia Indicates Links Between Bacterial Tyrosine Biosynthesis and Cognitive Dysfunction. Biological psychiatry global open science. 2022;3(2)283–291. https://doi.org/10.1016/j.bpsgos.2022.01.009
15. Wang Z, Yuan X, Zhu Z, Pang L, Ding S, Li X, Kang Y, Hei G, Zhang L, Zhang X, Wang S, Jian X, Li Z, Zheng C, Fan X, Hu S, Shi Y, Song X. Multiomics Analyses Reveal Microbiome-Gut-Brain Crosstalk Centered on Aberrant Gamma-Aminobutyric Acid and Tryptophan Metabolism in Drug-Naïve Patients with First-Episode Schizophrenia. Schizophr Bull. 2024;50(1):187–98. https://doi.org/10.1093/schbul/sbad026.
16. Tomasik J, Yolken RH, Bahn S, Dickerson FB. Immunomodulatory Effects of Probiotic Supplementation in Schizophrenia Patients: A Randomized, Placebo-Controlled Trial. Biomarker insights. 2015;10:47–54. https://doi.org/10.4137/BMI.S22007.
17. Okubo R, Koga M, Katsumata N, Odamaki T, Matsuyama S, Oka M, Narita H, Hashimoto N, Kusumi I, Xiao J, Matsuoka YJ. Effect of bifidobacterium breve A-1 on anxiety and depressive symptoms in schizophrenia: A proof-of-concept study. J Affect Disord. 2019;245:377–85. https://doi.org/10.1016/j.jad.2018.11.011.
18. Wan Z, Zhang X, Jia X, Qin Y, Sun N, Xin J, Zeng Y, Jing B, Fang J, Pan K, Zeng D, Bai Y, Wang H, Ma H, Ni X. Lactobacillus johnsonii YH1136 plays a protective role against endogenous pathogenic bacteria induced intestinal dysfunction by reconstructing gut microbiota in mice exposed at high altitude. Front Immunol. 2022;13:1007737. https://doi.org/10.3389/fimmu.2022.1007737.
19. Lee HJ, Lim SM, Kim DH. Lactobacillus johnsonii CJLJ103 Attenuates Scopolamine-Induced Memory Impairment in Mice by Increasing BDNF Expression and Inhibiting NF-κB Activation. J Microbiol Biotechnol. 2018;28(9):1443–6. https://doi.org/10.4014/jmb.1805.05025.
20. Wang H, He S, Xin J, Zhang T, Sun N, Li L, Ni X, Zeng D, Ma H, Bai Y. Psychoactive Effects of Lactobacillus johnsonii Against Restraint Stress-Induced Memory Dysfunction in Mice Through Modulating Intestinal Inflammation and permeability-a Study Based on the Gut-Brain Axis Hypothesis. Front Pharmacol. 2021;12: 662148. https://doi.org/10.3389/fphar.2021.662148.
21. Sun N, Ni X, Wang H, Xin J, Zhao Y, Pan K, Jing B, Zeng D. Probiotic Lactobacillus johnsonii BS15 Prevents Memory Dysfunction Induced by Chronic High-Fluorine Intake through Modulating Intestinal Environment and Improving Gut Development. Probiotics and antimicrobial proteins. 2020;12(4):1420–38. https://doi.org/10.1007/s12602-020-09644-9.
22. Kruk-Slomka M, Biala G. Cannabidiol Attenuates MK-801-Induced Cognitive Symptoms of Schizophrenia in the Passive Avoidance Test in Mice. Molecules (Basel, Switzerland). 2021;26(19):5977. https://doi.org/10.3390/molecules26195977.
23. Zhao J, Liu X, Huo C, Zhao T, Ye H. Abnormalities in Prefrontal Cortical Gene Expression Profiles Relevant to Schizophrenia in MK-801-Exposed C57BL/6 Mice. Neuroscience. 2018;390:60–78. https://doi.org/10.1016/j.neuroscience.2018.07.046.
24. Jeong Y, Bae HJ, Park K, Bae HJ, Yang X, Cho YJ, Jung SY, Jang DS, Ryu JH. 4-Methoxycinnamic acid attenuates schizophrenia-like behaviors induced by MK-801 in mice. J Ethnopharmacol. 2022;285: 114864. https://doi.org/10.1016/j.jep.2021.114864.
25. Akosman MS, Türkmen R, Demirel HH. Investigation of the protective effect of resveratrol in an MK-801-induced mouse model of schizophrenia. Environ Sci Pollut Res Int. 2021;28(46):65872–84. https://doi.org/10.1007/s11356-021-15664-x.
26. Xin J, Zeng D, Wang H, Sun N, Khalique A, Zhao Y, Wu L, Pan K, Jing B, Ni X. Lactobacillus johnsonii BS15 improves intestinal environment against fluoride-induced memory impairment in mice-a study based on the gut-brain axis hypothesis. PeerJ. 2020;8: e10125. https://doi.org/10.7717/peerj.10125.
27. Zhu, F., Guo, R., Wang, W., Ju, Y., Wang, Q., Ma, Q., Sun, Q., Fan, Y., Xie, Y., Yang, Z., Jie, Z., Zhao, B., Xiao, L., Yang, L., Zhang, T., Liu, B., Guo, L., He, X., Chen, Y., Chen, C., … Ma, X. Transplantation of microbiota from drug-free patients with schizophrenia causes schizophrenia-like abnormal behaviors and dysregulated kynurenine metabolism in mice. Molecular psychiatry. 2020;25(11)2905–2918. https://doi.org/10.1038/s41380-019-0475-4
28. Areal LB, Herlinger AL, Pelição FS, Martins-Silva C, Pires RGW. Crack cocaine inhalation induces schizophrenia-like symptoms and molecular alterations in mice prefrontal cortex. J Psychiatr Res. 2017;91:57–63. https://doi.org/10.1016/j.jpsychires.2017.03.005.
29. Xin J, Zhu B, Wang H, Zhang Y, Sun N, Cao X, Zheng L, Zhou Y, Fang J, Jing B, Pan K, Zeng Y, Zeng D, Li F, Xia Y, Xu P, Ni X. Prolonged fluoride exposure induces spatial-memory deficit and hippocampal dysfunction by inhibiting small heat shock protein 22 in mice. J Hazard Mater. 2023;456:131595. https://doi.org/10.1016/j.jhazmat.2023.131595.
30. Bolyen, E., Rideout, J. R., Dillon, M. R., Bokulich, N. A., Abnet, C., Al-Ghalith, G. A., et al. QIIME 2: Reproducible, interactive, scalable, and extensible microbiome data science. Peer J Preprints. 2018;6:e27295v2. https://doi.org/10.7287/peerj.preprints27295v2
31. Callahan BJ, McMurdie PJ, Rosen MJ, Han AW, Johnson AJ, Holmes SP. DADA2: High-resolution sample inference from Illumina amplicon data. Nat Methods. 2016;13(7):581–3. https://doi.org/10.1038/nmeth.3869.
32. Price MN, Dehal PS, Arkin AP. FastTree: computing large minimum evolution trees with profiles instead of a distance matrix. Mol Biol Evol. 2009;26(7):1641–50. https://doi.org/10.1093/molbev/msp077.
33. Bars-Cortina D, Moratalla-Navarro F, García-Serrano A, Mach N, Riobó-Mayo L, Vea-Barbany J, Rius-Sansalvador B, Murcia S, Obón-Santacana M, Moreno V. Improving Species Level-taxonomic Assignment from 16S rRNA Sequencing Technologies. Current protocols. 2023;3(11): e930. https://doi.org/10.1002/cpz1.930.
34. Herrera-deGuise C, Varela E, Sarrabayrouse G, Pozuelo Del Río M, Alonso VR, Sainz NB, Casellas F, Mayorga LF, Manichanh C, Vidaur FA, Guarner F. Gut Microbiota Composition in Long-Remission Ulcerative Colitis is Close to a Healthy Gut Microbiota. Inflamm Bowel Dis. 2023;29(9):1362–9. https://doi.org/10.1093/ibd/izad058.
35. Bray J, Curtis J. An ordination of the upland forest communities of Southern Wisconsin. Ecol Monogr. 1957;27:325–49.
36. Zeineldin M, Lowe J, Aldridge B. Effects of Tilmicosin Treatment on the Nasopharyngeal Microbiota of Feedlot Cattle With Respiratory Disease During the First Week of Clinical Recovery. Frontiers in veterinary science. 2020;7:115. https://doi.org/10.3389/fvets.2020.00115.
37. Dai, T., Zhang, Y., Tang, Y., Bai, Y., Tao, Y., Huang, B., & Wen, D. Identifying the key taxonomic categories that characterize microbial community diversity using full-scale classification: a case study of microbial communities

in the sediments of Hangzhou Bay. FEMS microbiology ecology. 2017;93(1), fiw203. https://doi.org/10.1093/femsec/fiw203
38. Severns PM, Sykes EM. Indicator Species Analysis: A Useful Tool for Plant Disease Studies. Phytopathology. 2020;110(12):1860–2. https://doi.org/10.1094/PHYTO-12-19-0462-LE.
39. Gweon HS, Bowes MJ, Moorhouse HL, Oliver AE, Bailey MJ, Acreman MC, Read DS. Contrasting community assembly processes structure lotic bacteria metacommunities along the river continuum. Environ Microbiol. 2021;23(1):484–98. https://doi.org/10.1111/1462-2920.15337.
40. Deng Y, Jiang YH, Yang Y, He Z, Luo F, Zhou J. Molecular ecological network analyses BMC bioinformatics. 2012;13:113. https://doi.org/10.1186/1471-2105-13-113.
41. Hu Y, Wang H, Jia H, Pen M, Liu N, Wei J, Zhou B. Ecological Niche and Interspecific Association of Plant Communities in Alpine Desertification Grasslands: A Case Study of Qinghai Lake Basin. Plants (Basel, Switzerland). 2022;11(20):2724. https://doi.org/10.3390/plants11202724.
42. Douglas GM, Maffei VJ, Zaneveld JR, Yurgel SN, Brown JR, Taylor CM, Huttenhower C, Langille MGI. PICRUSt2 for prediction of metagenome functions. Nat Biotechnol. 2020;38(6):685–8. https://doi.org/10.1038/s41587-020-0548-6.
43. Lv S, Zhang X, Feng Y, Jiang Q, Niu C, Yang Y, Wang X. Gut Microbiota Combined With Metabolomics Reveals the Repeated Dose Oral Toxicity of β-Cyclodextrin in Mice. Front Pharmacol. 2021;11: 574607. https://doi.org/10.3389/fphar.2020.574607.
44. Yang QJ, Zhao JR, Hao J, Li B, Huo Y, Han YL, Wan LL, Li J, Huang J, Lu J, Yang GJ, Guo C. Serum and urine metabolomics study reveals a distinct diagnostic model for cancer cachexia. J Cachexia Sarcopenia Muscle. 2018;9(1):71–85. https://doi.org/10.1002/jcsm.12246.
45. Kanehisa M, Furumichi M, Sato Y, Kawashima M, Ishiguro-Watanabe M. KEGG for taxonomy-based analysis of pathways and genomes. Nucleic Acids Res. 2023;51(D1):D587–92. https://doi.org/10.1093/nar/gkac963.
46. Zhao J, He K, Du H, Wei G, Wen Y, Wang J, Zhou X, Wang J. Bioinformatics prediction and experimental verification of key biomarkers for diabetic kidney disease based on transcriptome sequencing in mice. PeerJ. 2022;10: e13932. https://doi.org/10.7717/peerj.13932.
47. Mazhar SH, Li X, Rashid A, Su J, Xu J, Brejnrod AD, Su JQ, Wu Y, Zhu YG, Zhou SG, Feng R, Rensing C. Co-selection of antibiotic resistance genes, and mobile genetic elements in the presence of heavy metals in poultry farm environments. The Science of the total environment. 2021;755(Pt 2): 142702. https://doi.org/10.1016/j.scitotenv.2020.142702.
48. Abdi, Hervé, Williams, L. J., & Valentin, D. Multiple factor analysis: principal component analysis for multitable and multiblock data sets. Wiley Interdisciplinary Reviews: Computational Statistics. 2013;(2)149–179. https://doi.org/10.1002/wics.1246
49. Noecker C, Eng A, Muller E, Borenstein E. MIMOSA2: a metabolic network-based tool for inferring mechanism-supported relationships in microbiome-metabolome data. Bioinformatics (Oxford, England). 2022;38(6):1615–23. https://doi.org/10.1093/bioinformatics/btac003.
50. Picart-Armada S, Fernández-Albert F, Vinaixa M, Yanes O, Perera-Lluna A. FELLA: an R package to enrich metabolomics data. BMC Bioinformatics. 2018;19(1):538. https://doi.org/10.1186/s12859-018-2487-5.
51. Yu, G., Xu, C., Zhang, D., Ju, F., & Ni, Y. MetOrigin: Discriminating the origins of microbial metabolites for integrative analysis of the gut microbiome and metabolome. iMeta. 2022;1(1)e10. https://doi.org/10.1002/imt2.10
52. Kerseviciute, I., & Gordevicius, J. aPEAR: an R package for autonomous visualization of pathway enrichment networks. Bioinformatics (Oxford, England).2023;39(11), btad672. https://doi.org/10.1093/bioinformatics/btad672
53. Mañé J, Lorén V, Pedrosa E, Ojanguren I, Xaus J, Cabré E, Domènech E, Gassull MA. Lactobacillus fermentum CECT 5716 prevents and reverts intestinal damage on TNBS-induced colitis in mice. Inflamm Bowel Dis. 2009;15(8):1155–63. https://doi.org/10.1002/ibd.20908.
54. Jones CA, Watson DJ, Fone KC. Animal models of schizophrenia. Br J Pharmacol. 2011;164(4):1162–94. https://doi.org/10.1111/j.1476-5381.2011.01386.x.
55. Liang JQ, Chen X, Cheng Y. Paeoniflorin Rescued MK-801-Induced Schizophrenia-Like Behaviors in Mice via Oxidative Stress Pathway. Front Nutr. 2022;9: 870032. https://doi.org/10.3389/fnut.2022.870032.
56. Senkowski D, Gallinat J. Dysfunctional prefrontal gamma-band oscillations reflect working memory and other cognitive deficits in schizophrenia. Biol Psychiat. 2015;77(12):1010–9. https://doi.org/10.1016/j.biopsych.2015.02.034.
57. Galey D, Jaffard R, Le Moal M. Spontaneous alternation disturbance after lesions of the ventral mesencephalic tegmentum in the rat. Neurosci Lett. 1976;3(1–2):65–9. https://doi.org/10.1016/0304-3940(76)90101-4.
58. Favalli G, Li J, Belmonte-de-Abreu P, Wong AH, Daskalakis ZJ. The role of BDNF in the pathophysiology and treatment of schizophrenia. J Psychiatr Res. 2012;46(1):1–11. https://doi.org/10.1016/j.jpsychires.2011.09.022.
59. Han M, Deng C. BDNF as a pharmacogenetic target for antipsychotic treatment of schizophrenia. Neurosci Lett. 2020;726: 133870. https://doi.org/10.1016/j.neulet.2018.10.015.
60. Yang, P., Huang, S., Luo, Z., Zhou, S., Zhang, C., Zhu, Y., Yang, J., & Li, L. Radix Bupleuri aqueous extract attenuates MK801-induced schizophrenia-like symptoms in mice: Participation of intestinal flora. Biomedicine & pharmacotherapy = Biomedecine & pharmacotherapie. 2024;172:116267. https://doi.org/10.1016/j.biopha.2024.116267
61. Kocsis B. Differential role of NR2A and NR2B subunits in N-methyl-D-aspartate receptor antagonist-induced aberrant cortical gamma oscillations. Biol Psychiatry. 2012;71(11):987–95. https://doi.org/10.1016/j.biopsych.2011.10.002.
62. Kristiansen, L. V., Patel, S. A., Haroutunian, V., & Meador-Woodruff, J. H. Expression of the NR2B-NMDA receptor subunit and its Tbr-1/CINAP regulatory proteins in postmortem brain suggest altered receptor processing in schizophrenia. Synapse (New York, N.Y.). 2010;64(7)495–502. https://doi.org/10.1002/syn.20754
63. Kanchanatawan B, Hemrungrojn S, Thika S, Sirivichayakul S, Ruxrungtham K, Carvalho AF, Geffard M, Anderson G, Maes M. Changes in Tryptophan Catabolite (TRYCAT) Pathway Patterning Are Associated with Mild Impairments in Declarative Memory in Schizophrenia and Deficits in Semantic and Episodic Memory Coupled with Increased False-Memory Creation in Deficit Schizophrenia. Mol Neurobiol. 2018Jun;55(6):5184–201. https://doi.org/10.1007/s12035-017-0751-8.
64. Deng H, He L, Wang C, Zhang T, Guo H, Zhang H, Song Y, Chen B. Altered gut microbiota and its metabolites correlate with plasma cytokines in schizophrenia inpatients with aggression. BMC Psychiatry. 2022;22(1):629. https://doi.org/10.1186/s12888-022-04255-w.
65. Xiang M, Zheng L, Pu D, Lin F, Ma X, Ye H, Pu D, Zhang Y, Wang D, Wang X, Zou K, Chen L, Zhang Y, Sun Z, Zhang T, Wu G. Intestinal Microbes in Patients With Schizophrenia Undergoing Short-Term Treatment: Core Species Identification Based on Co-Occurrence Networks and Regression Analysis. Front Microbiol. 2022;13: 909729. https://doi.org/10.3389/fmicb.2022.909729.
66. Dickerson, F. B., Stallings, C., Origoni, A., Katsafanas, E., Savage, C. L., Schweinfurth, L. A., Goga, J., Khushalani, S., & Yolken, R. H. Effect of probiotic supplementation on schizophrenia symptoms and association with gastrointestinal functioning: a randomized, placebo-controlled trial. The primary care companion for CNS disorders. 2014;16(1)PCC.13m01579. https://doi.org/10.4088/PCC.13m01579
67. Fan Y, Gao Y, Ma Q, Yang Z, Zhao B, He X, Yang J, Yan B, Gao F, Qian L, Wang W, Zhu F, Ma X. Multi-Omics Analysis Reveals Aberrant Gut-Metabolome-Immune Network in Schizophrenia. Front Immunol. 2022;13: 812293. https://doi.org/10.3389/fimmu.2022.812293.
68. Fan, K. Q., Li, Y. Y., Wang, H. L., Mao, X. T., Guo, J. X., Wang, F., Huang, L. J., Li, Y. N., Ma, X. Y., Gao, Z. J., Chen, W., Qian, D. D., Xue, W. J., Cao, Q., Zhang, L., Shen, L., Zhang, L., Tong, C., Zhong, J. Y., Lu, W., … Jin, J. Stress-Induced Metabolic Disorder in Peripheral CD4+ T Cells Leads to Anxiety-like Behavior. Cell. 2019;179(4)864–879.e19. https://doi.org/10.1016/j.cell.2019.10.001
69. Li S, Zhuo M, Huang X, Huang Y, Zhou J, Xiong D, Li J, Liu Y, Pan Z, Li H, Chen J, Li X, Xiang Z, Wu F, Wu K. Altered gut microbiota associated with symptom severity in schizophrenia. PeerJ. 2020;8: e9574. https://doi.org/10.7717/peerj.9574.
70. Borkent J, Ioannou M, Laman JD, Haarman BCM, Sommer IEC. Role of the gut microbiome in three major psychiatric disorders. Psychol Med. 2022;52(7):1222–42. https://doi.org/10.1017/S0033291722000897.
71. Ghaderi A, Banafshe HR, Mirhosseini N, Moradi M, Karimi MA, Mehrzad F, Bahmani F, Asemi Z. Clinical and metabolic response to vitamin D plus probiotic in schizophrenia patients. BMC Psychiatry. 2019;19(1):77. https://doi.org/10.1186/s12888-019-2059-x.

72. Fine RL, Mubiru DL, Kriegel MA. Friend or foe? Lactobacillus in the context of autoimmune disease. Adv Immunol. 2020;146:29–56. https://doi.org/10.1016/bs.ai.2020.02.002.
73. Piraino S, Fanelli G, Boero F. Variability of species' roles in marine communities: change of paradigms for conservation priorities. Mar Biol. 2002;140(5):1067–74. https://doi.org/10.1007/s00227-001-0769-2.
74. Matchado MS, Lauber M, Reitmeier S, Kacprowski T, Baumbach J, Haller D, List M. Network analysis methods for studying microbial communities: A mini review. Comput Struct Biotechnol J. 2021;19:2687–98. https://doi.org/10.1016/j.csbj.2021.05.001.
75. De Cáceres M, Legendre P. Associations between species and groups of sites: indices and statistical inference. Ecology. 2009;90(12):3566–74. https://doi.org/10.1890/08-1823.1.
76. Wu, D., Jiao, N., Zhu, R., Zhang, Y., Gao, W., Fang, S., Li, Y., Cheng, S., Tian, C., Lan, P. Identification of the keystone species in non-alcoholic fatty liver disease by causal inference and dynamic intervention modeling. Gastroenterology. 2020;158(6), S-1412-S-1413. https://doi.org/10.1101/2020.08.06.240655
77. Yu, J., Sun, J., Sun, M., Li, W., Qi, D., Zhang, Y. & Han C. Protective mechanism of Coprinus comatus polysaccharide on acute alcoholic liver injury in mice, the metabolomics and gut microbiota investigation. Food Science and Human Wellness. 2024;13(01):401–413.
78. Gu M, Li C, Chen L, Li S, Xiao N, Zhang D, Zheng X. Insight from untargeted metabolomics: Revealing the potential marker compounds changes in refrigerated pork based on random forests machine learning algorithm. Food Chem. 2023;424: 136341. https://doi.org/10.1016/j.foodchem.2023.136341.
79. Li, Y., Wang, L., Wang, H., Leng, X., Gao, J., & Huang, D. Polysaccharides from Eucommia ulmoides Oliv. leaves alleviates alcohol-induced mouse brain injury and BV-2 microglial dysfunction. International journal of biological macromolecules. 2024;273(Pt 1)132887. https://doi.org/10.1016/j.ijbiomac.2024.132887
80. Karim, M., & Wang, B. Is sialic acid in milk food for the brain?. CAB Reviews Perspectives in Agriculture Veterinary ence Nutrition and Natural Resources. 2006;1(18). https://doi.org/10.1079/PAVSNNR20061018
81. Suzzi, S., Croese, T., Ravid, A., Gold, O., Clark, A. R., Medina, S., Kitsberg, D., Adam, M., Vernon, K. A., Kohnert, E., Shapira, I., Malitsky, S., Itkin, M., Brandis, A., Mehlman, T., Salame, T. M., Colaiuta, S. P., Cahalon, L., Slyper, M., Greka, A., Schwartz, M. N-acetylneuraminic acid links immune exhaustion and accelerated memory deficit in diet-induced obese Alzheimer's disease mouse model. Nature communications. 2023l;14(1)1293. https://doi.org/10.1038/s41467-023-36759-8
82. Cui G, Qing Y, Li M, Sun L, Zhang J, Feng L, Li J, Chen T, Wang J, Wan C. Salivary Metabolomics Reveals that Metabolic Alterations Precede the Onset of Schizophrenia. J Proteome Res. 2021;20(11):5010–23. https://doi.org/10.1021/acs.jproteome.1c00504.

Publisher's Note